Unraveling the conundrum of river response to rising sea level from laboratory to field. Part II. The Fly-Strickland River System, Papua New Guinea

GARY PARKER[a], TETSUJI MUTO[b], YOSHIHISA AKAMATSU[c], WILLIAM E. DIETRICH[d] and J. WESLEY LAUER[e]

[a]*Dept. of Civil and Environmental Engineering and Dept. of Geology, University of Illinois, Hydrosystems Laboratory, 205 N. Mathews, Urbana Illinois 61801 USA.*
[b]*Faculty of Environmental Studies, Nagasaki University, 1-14 Bunkyomachi, Nagasaki 852-8521, Japan*
[c]*Department of Environmental Science and Technology, Tokyo Institute of Technology 4259, Nagatsuda-cho, Midori-ku, Yokohama-shi, Kanagawa, 226-8502, Japan*
[d]*Department of Earth and Planetary Science, University of California Berkeley, CA 94720-4767 USA*
[e]*St. Anthony Falls Laboratory, University of Minnesota, 2 3rd St. SE, Minneapolis, MN 55141 USA.*

ABSTRACT

The most recent deglaciation resulted in a global sea level rise of some 120 m over approximately 12000 years. A moving boundary numerical model is developed to predict the response of rivers to this rise. The model was motivated by experiments at small-scale, which have identified two modes describing the transgression of a river mouth: autoretreat without abandonment of the river delta (no sediment starvation at the topset-foreset break) and sediment-starved autoretreat with abandonment of the delta. In the latter case transgression is far more rapid, and its effects are felt much farther upstream of the river mouth. A moving boundary numerical model that captures these features in experimental deltas is adapted to describe the response of the Fly-Strickland River system, Papua New Guinea. In the absence of better information, the model is applied to the case of sea level rise without local climate change in New Guinea. The model suggests that a) sea level rise forced the river mouth to transgress over 700 km since the last glacial maximum, b) sediment-starved autoretreat forced enough bed aggradation to block a tributary with a low sediment load and create the present-day Lake Murray, c) the resulting aggradation was sufficient to move the gravel-sand transition on the Strickland River upstream, d) the present-day Fly Estuary may be in part a relict river valley drowned by sea level rise and partially filled by tidal effects, and e) the Fly River is presently reforming its bankfull geometry and prograding into the Fly Estuary. A parametric study with the model indicates that sediment concentration during floods plays a key role in determining whether or not, and to what extent, transgression is expressed in terms of sediment-starved autoretreat. A sufficiently high sediment concentration can prevent sediment-starved autoretreat during the entire sea level cycle. This observation may explain why some present-day river mouths are expressed in terms of deltas protruding into the sea, and others are wholly contained within embayments or estuaries in which water has invaded landward.

Keywords rivers, deltas, transgression, sea level, autoretreat

INTRODUCTION

This paper is a companion to Parker *et al*. (submitted); both papers address the response of rivers to sea level rise. The last deglaciation caused a

Pleistocene-Holocene eustatic sea level rise of some 120 m. Nearly all this rise was realized in a 12000 period between 18000 and 6000 years BP. Sea level rise likely had a dramatic effect on rivers near their mouths, and perhaps farther upstream.

In the companion paper, Parker *et al*. (submitted), a numerical model of delta response to sea level rise is outlined and tested against the experiments of Muto (2001). The numerical successfully captures two modes of shoreline transgression identified by Muto (2001); autoretreat without abandonment of the river delta (no sediment starvation at the topset-foreset break) and sediment-starved autoretreat with abandonment of the delta. Here the model is adapted to study the effect of Holocene sea level rise on the Fly-Strickland River system, Papua New Guinea.

THE FLY-STRICKLAND RIVER SYSTEM, PAPUA NEW GUINEA

Overview The Fly-Strickland River system is a major river system that drains the tectonically active highlands of New Guinea, crosses the Fly Platform and flows into the Gulf of Papua (Fig. 1). The lower Fly River is the reach below Everill Junction (Fig. 1). Everill Junction is formed by the confluence of the middle Fly River from the west and the larger Strickland River from the east (Fig. 2). The total area drained by the system is about 75,000 km^2.

In the highlands both the Fly and Strickland Rivers alternate between bedrock and gravel-bed morphologies in response to a complex pattern of uplift. As they flow onto the lower slopes of the Fly Platform they become alluvial gravel-bed streams. Farther downstream both streams undergo a transition from gravel-bed to sand-bed morphology. The transition points appear to fall near a hinge line, with uplift to the northeast and slow subsidence to the southwest (Dietrich et al., 1999). Of prime interest here are the sand-bed reaches.

Three abbreviations appear in Figure 1. “EFR” denotes the downstream end of the fluvial reach, beyond which the channel widens considerably into an estuary. “BEF” denotes the upstream end, or beginning point downstream of which the estuary rapidly flares outward. “OEE” denotes the outer edge of the estuary. These points are referenced later in the paper.

Blocked-valley lakes: a relict of Pleistocene-Holocene sea level rise A characteristic feature of the sand-bed Fly and Strickland Rivers above Everill Junction is the presence of numerous blocked-valley lakes, the largest of which is Lake Murray (Fig. 2). These lakes appear to have formed in response to Pleistocene-Holocene sea level rise (Pickup, 1984; Dietrich et al., 1999). That is, sea level rise forced aggradation on the main-stem Fly and Strickland Rivers, both of which have sediment supplies sourced in the highlands. The small tributaries flowing into the Fly and Strickland Rivers in Fig. 15 are not sourced in the highlands, and as a result have much lower sediment yields per unit drainage area. As a result they were not able to aggrade in pace with main-stem aggradation, so resulting in the blocked-valley lakes (Pickup,1984; Dietrich et al.,1999).

Effect of climate change The most extensive available studies of the effect of sea level rise on large, lowland streams have been conducted on rivers at relatively high latitudes which are subject to a temperate climate under present-day conditions. Two examples discussed in Blum and Törnqvist (2000) are those of the Mississippi and Rhine Rivers. While sea level rise itself is an upstream-propagating consequence of deglaciation, such rivers were also subjected to downstream-propagating effects associated with deglaciation. These include meltwater floods that were at times orders of magnitude larger than the floods experienced today, and sediment loads derived from glacial till which may also have been considerably higher than those experienced in the present. The combination of both upstream- and downstream-propagating effects makes the direct signature of sea level rise rather difficult to discern.

The island of New Guinea offers an obvious advantage in this regard. New Guinea undoubtedly underwent a noticeable change in climate from the last glacial maximum to the present. This change is evidenced by, among other things, a dramatic reduction in glaciated area in the highlands from the last glacial maximum to the present (Hope and Peterson, 1975; Peterson et al., 2002). This comment notwithstanding, even at the last glacial maximum the areal fraction of the highlands that was actually glaciated in no way compares with the coverage of North America and Europe by continental glaciers. More precisely, the country of Papua New Guinea occupying the eastern half of the island has an area near 475,000 km^2, of which perhaps less than 1000 km^2 were glaciated during the last glacial maximum (e.g. Peterson et al., 2002). Located at the equator and surrounded by the Pacific Ocean, it can be surmised that climate variation from the last glacial maximum to the present was much weaker than at higher latitudes (e.g. Loffler, 1973), and that glacial outburst floods similarly played a much smaller role.

In the absence of more precise information, then, the following very crude approximations are nevertheless reasonable for the case of the Fly-Strickland River system in Papua New Guinea:

- Local climate, and in particular hydrologic regime and sediment production rates are taken to be constant from the last glacial maximum to the present: and
- the effect of change in conditions from the last glacial maximum to present day is expressed solely in terms of the direct upstream-propagating effect of 120 m of eustatic sea level rise.

These assumptions can be modified appropriately as better information is obtained about climate change in Papua New Guinea.

Discharge and long profiles of the Fly-Strickland River system

Documentation concerning the Fly-Strickland River system is available largely due to the needs of two mines, i.e. the Ok Tedi copper mine near the headwaters of the Ok Tedi, a tributary of the Fly River, and the Porgera gold mine near the headwaters of the Strickland River. Two of the authors (Dietrich and Parker) have served as long-term consultants to the Ok Tedi mine, and one (Parker) has served as a long-term consultant to the Porgera mine. Data obtained from these sources are extensively used in this paper (e.g. Cui and Parker, 1999).

The Middle Fly River between D'Albertis Junction and Everill Junction has a downchannel length of about 450 km (Figs. 1, 2). A number of smaller tributaries, but no major tributaries enter this reach. As a result the mean annual discharge increases only from about 1900 m^3/s at D'Albertis Junction to about 2250 m^3/s at Everill Junction (Higgins, 1990). At present this reach of the river is affected by sediment input from a mine. Under pre-mine conditions, however, it is estimated that the mean annual sediment discharge increased only from 6.9 million tons per year at D'Albertis Junction to 8.0 million tons per year at Everill Junction. The Fly River has a sand bed throughout this reach.

Discharges on the Strickland River upstream of Everill Junction are less well documented. The mean annual discharge at Everill Junction is on the order of 3100 m^3/s (e.g. Higgins, 1990). The floodplain of the Strickland River is shown in Fig. 3; a transition from gravel-bed to sand-bed morphology is located about 269 km up-channel from Everill Junction. The Strickland River is estimated to carry an annual load near 70 million tons per year at Everill Junction (Dietrich *et al.,* 1999).

Both the Fly and Strickland Rivers are large tropical rivers characterized by a remarkably small variation in flow discharge. As a result the rivers tend to be in flood for as much as 10% to 40% of the time, and bankfull discharge is only modestly higher than mean annual discharge (Pickup, 1984; Dietrich *et al.*, 1999).

Long profiles of the Strickland and Fly Rivers upstream of Everill Junction are given in Fig. 14. The slope of the Middle Fly River near Everill Junction is near $1x10^{-5}$; the corresponding values for the sand-bed and gravel-bed Strickland River reaches are near $1.0x10^{-4}$ and $4.6x10^{-4}$, respectively. The much higher slope of the sand-bed Strickland River as compared to the sand-bed Middle Fly

River reflects the much higher (and coarser) sediment load. The Fly River from Everill Junction to the point where the estuary starts to flare out (BEF, or "beginning of estuary flare" in Fig. 13) has a downchannel length of about 290 km and an average slope of ~ 1.5×10^{-5}.

Abstraction for the purpose of numerical modeling In so far as the Strickland River is the dominant branch of the Fly River upstream of D'Albertis Junction, the river system is simplified in the following way. A single stem with no tributaries extends from the Gulf of Papua upstream to Everill Junction, and then follows the Strickland River to the gravel-sand transition. For simplicity the gravel-sand transition is replaced with a bedrock-sand transition. While much of the Fly Platform below a line passing through the gravel-sand transitions of the Fly and Strickland Rivers appears to be slowly subsiding, the rate of subsidence appears to be low enough to justify its neglect relative to the sea level rise at an average rate of 10 mm/year experienced over the 12000-year period between 18000 and 6000 years BP.

Like most large sand-bed rivers, both the Fly and Strickland Rivers show a general pattern of downstream fining of characteristic grain size (e.g. Wright and Parker, 2004a,b). It is possible to incorporate this fining into a model of the effect of sea level rise on a large sand-bed river (Wright and Parker, 2005a,b). Here, however, the size distribution of the sand is abstracted to a single grain size, and downstream fining is not modeled.

Many river systems may not have maintained the same planform morphology throughout Pleistocene-Holocene sea level rise. For example, the lower Mississippi River, which is a meandering stream today, may have been a braided stream during the early stages of Pleistocene-Holocene sea level rise (Fisk, 1944). In the present analysis, however, it is assumed that the planform of the Fly-Strickland River System remained in the meandering state throughout Pleistocene-Holocene sea level rise. This assumption is consistent with the assumptions of constant regimes of hydrology and sediment yield introduced earlier. The calculations presented below provide some *a posteriori* evidence in justification of the assumption of a sustained meandering planform

ADAPTATION OF THE NUMERICAL MODEL TO THE FLY-STRICKLAND RIVER SYSTEM

Overview of the adaptations The overall structure of the numerical model used to study the response of the experimental model of Muto (2001) to base level rise is directly applicable to field rivers. A number of modules within this basic structure must, however, be changed in order to allow adaptation to realistic field conditions. These are enumerated below.

- *Flow intermittency* In the experiments of Muto (2001), the water discharge and sediment feed rate were held constant for the duration of the experiments. Rivers, however, alternate between flood flows and low flows, and tend to be morphologically inactive at low flows.
- *Characterization of sand transport* Equation (1) is applicable only to the experiments of Muto (2001), and must be replaced by an equation known to be appropriate for sand-bed rivers in application to the field.

- *Self-formed channel* In the experiments of Muto (2001) the width of the flow was set by the experimenter. Rivers, however, are the authors of their own bankfull geometry.
- *Backwater* In contrast to the experiments of Muto (2001), in large, sand-bed rivers the Froude number at flood flow is usually sufficiently low to ensure that backwater effects extend far upstream of the zone of standing water.
- *Floodplain construction and wash load* In the experiments of Muto (2001) the channel was straight and had no floodplain, and the sediment feed and deposit were composed purely of sand. Sand-bed rivers are typically sinuous and have well-developed floodplains. They often transport more mud (silt and clay) than sand on an annual basis. This mud is typically transported as wash load, i.e. material that is in transport but does not deposit on the channel bed. Wash load does, however, deposit on the floodplain.
- *Differentiation between subaerial and subaqueous basement profiles* In the experiments of Muto (2001) the model bedrock basement had a constant slope S_b along which both the subaerial bedrock-alluvial transition and the foreset-subaqueous basement transition migrated (Fig. 5). In large rivers, however, it can be expected that the subaerial bedrock basement has a slope that differs from that of the subaqueous basement.
- *Decoupling of shoreline water surface elevation and elevation of topset-foreset break* In the experiments of Muto (2001), the flow depth was so

small that the elevation of the topset-foreset break could be approximated as equal to that of the water surface immediately above it. The position of both could be identified with the shoreline as long as the river mouth had not entered sediment-starved autoretreat. When backwater effects are included, however, the elevation of the topset-foreset break and the elevation of standing water above it become decoupled, even when the river mouth is not undergoing autoretreat.

Each of these items is considered in more detail below.

Intermittency In principle flow discharge should be represented in terms of a full annual hydrograph, with a corresponding variation of sediment feed at the upstream end. The same hydrograph could be repeated annually, or be allowed to vary according to e.g. a Monte Carlo scheme. Its characteristics could be varied in the long term as a proxy for climate change. Here, however, a simple constant intermittency I_f is used (Paola *et al.*, 1992). That is, the river is approximated as in flood and morphologically active for fraction I_f of time, during which the water discharge (volume water transported per unit time) is approximated as bankfull discharge Q_{bf}. The volume sand feed rate (sand only, excluding pores) per unit time during floods is denoted as Q_{sbff}. The river is assumed to be inactive when not in flood, and I_f is adjusted so that the annual average volume feed rate of sand is estimated by $I_f Q_{sbff}$ (Wright and Parker, 2005a,b).

Characterization of sand transport Sand transport is characterized in terms of the sediment transport equation of Engelund and Hansen (1967), a relation that is known to have applicability to rivers in addition to experimental flumes (Brownlie, 1981). The relation takes the form

$$q^* = \frac{0.05}{C_f}(\tau^*)^{5/2} \tag{1}$$

In the above equation q* denotes the dimensionless Einstein number characterizing sediment transport rate, τ* denotes the dimensionless Shields number characterizing bed shear stress and C_f is a dimensionless coefficient of bed friction, defined respectively as

$$q^* = \frac{q_s}{\sqrt{RgD}\,D} \quad , \quad \tau^* = \frac{\tau_b}{\rho RgD} \quad , \quad C_f = \frac{\tau_b}{\rho U^2} \tag{2a,b,c}$$

In the above relation q_s denotes the volume sand transport rate (excluding pores) per unit width, D denotes characteristic sand grain size (e.g. median or geometric mean size), τ_b denotes the bed shear stress, U denotes the depth-averaged velocity of flow, ρ denotes water density, g denotes the acceleration of gravity and

$$R = \frac{\rho_s}{\rho} - 1 \tag{2d}$$

denotes the submerged specific gravity of the sediment, where ρ_s denotes sediment density. In the case of quartz, for example, R is near 1.65.

The sand transport relation of Engelund and Hansen (1967) is adequate for the present work, in which a single grain size D is assumed. A different relation would be necessary were the analysis to be extended to mixtures. Wright and Parker (2004a,b) provide such a formulation, and Wright and Parker

(2005a,b) apply this formulation to the problem of downstream fining large in sand-bed rivers.

Equation (1) requires a knowledge of the bed friction coefficient C_f, or alternatively the dimensionless Chezy friction coefficient Cz, where

$$Cz = C_f^{-1/2} \tag{3}$$

In the present analysis the Chezy friction coefficient at bankfull flow Cz_{bf} is approximated as a constant for a given river reach. Fig. 5 shows a plot of Cz_{bf} versus downchannel bed slope S for the compendium of sand-bed streams with values of grain size D less than 0.5 mm given in Parker et al. (1998) and the compendium of gravel-bed streams given in Parker and Toro-Escobar (2002). It is seen from the figure that sand-bed rivers tend to have values of Cz_{bf} between about 8 and 26, with the larger value corresponding to lower downchannel bed slope S. (The estimated point for the Strickland River is explained below.)

Self-formed channel A river constructs its own channel and floodplain. The characteristics of self-formed channels can be described in terms of bankfull parameters. Of interest here are bankfull depth H_{bf} and bankfull width B_{bf}. Now as an idealization consider a river in local equilibrium (locally graded river) with specified bankfull discharge Q_{bf}, volume sand transport at bankfull flow Q_{sbf}, bankfull Chezy resistance coefficient Cz_{bf}, characteristic grain size D and submerged specific gravity R. What would be the bankfull depth H_{bf}, bankfull width B_{bf} and downchannel bed slope S of the river?

Evidently three equations are needed to specify the three parameters. Before proceeding, however, it is necessary to introduce some standard conservation relations. The relation between total volume sand transport rate during floods Q_{sbf} and the corresponding volume sand transport rate (without pores) per unit width q_{sbf} is given by the conservation relation

$$Q_{sbf} = q_{sbf} B_{bf} \tag{4}$$

The relation between Q_{bf}, H_{bf} and depth-averaged flow velocity at bankfull flow U_{bf} is given by the conservation relation

$$Q_{bf} = U_{bf} B_{bf} H_{bf} \tag{5}$$

Finally, conservation of downchannel flow momentum at equilibrium (steady, uniform) bankfull flow requires a balance between the downstream force of gravity per unit bed area and the resistive force at the bed per unit area, so that where τ_{bbf} denotes the bankfull value of τ_b,

$$\tau_{bbf} = \rho g H_{bf} S \tag{6}$$

The first of the three relations needed to characterize the bankfull geometry of streams can be obtained by reducing the relation (6) describing momentum balance with (2c) and (5) to obtain

$$\left(\frac{\hat{Q}}{Cz_{bf} \hat{B} \hat{H}} \right)^2 = \hat{H} S \tag{7}$$

where $\hat{Q}$ denotes dimensionless bankfull discharge, $\hat{B}$ denotes dimensionless bankfull width and $\hat{H}$ denotes dimensionless bankfull depth, defined respectively as

$$\hat{Q} = \frac{Q_{bf}}{\sqrt{gD}\, D^2} \quad , \quad \hat{B} = \frac{B_{bf}}{D} \quad , \quad \hat{H} = \frac{H_{bf}}{D} \tag{8a,b,c}$$

The second relation is obtained by reducing the sand transport relation (1) with (2) – (8) to obtain

$$\hat{Q}_s = 0.05(Cz_{bf})^2 \hat{B} (\tau^*_{bf})^{5/2} \tag{9}$$

where

$$\hat{Q}_s = \frac{Q_{sbf}}{\sqrt{RgD}\,D^2} \quad , \quad \tau^*_{bf} = \frac{\hat{H}S}{R} \tag{10a,b}$$

denote the dimensionless sand transport rate at bankfull flow and the Shields number at bankfull flow, respectively.

Parker *et al.* (1998) follow the precedent of Paola et al. (1992) in specifying the third relation in terms of the empirical approximation of a constant "channel-forming" value of τ^*_{bf} here denoted as τ^*_{form}. That is, it is assumed that rivers co-evolve with their floodplains toward the attainment of an approximately constant value of bankfull Shields number:

$$\tau^*_{bf} \cong \tau^*_{form} \tag{11}$$

Parker *et al.* (1998) provide evidence for this for sand-bed streams with grain sizes less than 0.5 mm, and Parker and Toro-Escobar (2002) provide similar evidence for gravel-bed streams. The data in question are shown in Fig. 19. In the case of the sand-bed streams, the approximate specification of τ^*_{form} of 1.86 is yielded from the average of the sand-bed data in Fig. 6. (The estimated point for the Strickland River is explained below.)

Equations (7), (9) and (11) thus provide the three relations needed to solve for H_{bf}, B_{bf} and S for a channel in local equilibrium. These relations are found upon reduction to be

$$\hat{H} = \frac{0.05\,Cz_{bf}\,(\tau^*_{form})^2}{R^{1/2}}\frac{\hat{Q}}{\hat{Q}_s} \tag{12}$$

$$\hat{B} = \frac{\hat{Q}_s}{0.05\,Cz^2_{bf}\left(\tau^*_{form}\right)^{2.5}} \tag{13}$$

$$S = \frac{R^{3/2}}{0.05\,Cz_{bf}\,\tau^*_{form}}\frac{\hat{Q}_s}{\hat{Q}} \tag{14}$$

Equation (14) provides a sand transport relation for a self-formed channel transporting sediment in accordance with the transport equation of Engelund and Hansen (1967) at bankfull flow with constant bankfull Shields number. That is, rearranging (14),

$$\frac{Q_{sbf}}{Q_{bf}} = \frac{0.05\,Cz_{bf}\,\tau^*_{form}}{R^{3/2}}S \tag{15}$$

A comparison of (15) for field sand-bed rivers and (1) for the experiments of Muto (2001) indicates that the two relations at least have similar structures.

Backwater The treatment of the previous section is appropriate for river reaches in local equilibrium, in which backwater effects are sufficiently small to allow streamwise momentum balance to be approximated by (6). Sand-bed streams flowing into the sea are however, likely to be strongly affected by backwater, i.e. the upstream-propagating effect of ponded water. Backwater can be described by generalizing the statement of momentum balance of (6) to include quasi-steady pressure and inertial forces at bankfull flow. The appropriate relation is (e.g. Henderson, 1966)

$$U_{bf}\frac{dU_{bf}}{dx} + g\frac{dH_{bf}}{dx} = gS - \frac{\tau_{bbf}}{\rho H_{bf}} \tag{16a}$$

where x denotes a downchannel coordinate and S is given as

$$S = -\frac{\partial \eta}{\partial x} \tag{16b}$$

. Note that if the flow is spatially uniform the two terms on the left-hand side of (16a) vanish, and the equation reduces to (6).

In a channel of constant bankfull discharge Q_{bf} and bankfull width B_{bf}, the conservation equation (5) reduces to the form

$$q_{wbf} = U_{bf} H_{bf} = \text{const} \tag{17a}$$

where

$$q_{wbf} = Q_{bf} / B_{bf} \tag{17b}$$

denotes the water discharge per unit width at bankfull flow. Reducing (16a) with (17) and (2c) yields the standard backwater equation of open-channel flow (at bankfull conditions):

$$\left(1 - \mathbf{Fr}_{bf}^2\right)\frac{dH_{bf}}{dx} = S - S_{fric} \tag{18}$$

In the above equation S_{fric} denotes the bankfull friction slope, given as

$$S_{fric} = C_{fbf}\mathbf{Fr}_{bf}^2 \tag{19}$$

In addition, C_{fbf} denotes the bankfull value of C_f and $\mathbf{Fr}_{bf}$ denotes the dimensionless Froude number at bankfull flow, defined as

$$\mathbf{Fr}_{bf}^2 = \frac{q_{wbf}^2}{gH_{bf}^3} \tag{20}$$

Backwater effects can be neglected when the left-hand side of (18) is small compared to the right-hand side, in which case (18) can be reduced with the aid of (2c), (17) and (20) to the relation (6) describing momentum balance for normal flow. This is typically the case when the square of the Froude number in (18) is relatively high, i.e. near or above unity. While this was true for the experiments of Muto (2001), it is not the case for sand-bed rivers. Fig. 7 provides a plot of $\mathbf{Fr}_{bf}$ versus S for the same set of sand-bed and gravel-bed rivers as in Figs. 5 and 6. It is seen that $\mathbf{Fr}_{bf}$ can be as low as 0.2 for low-slope sand-bed rivers; the corresponding value of $\mathbf{Fr}_{bf}^2$ is 0.04. ((The estimated point for the Strickland River is explained below.)

The formulation of (18) is, however, not directly applicable to the case of self-formed sand-bed rivers considered here because of the assumption of constant channel width used in its derivation. It is thus necessary to return to the more primitive form (16a). Between (2b) and (2c) it is found that

$$\frac{U_{bf}}{\sqrt{RgD}} = \frac{\tau_{bf}^*}{\sqrt{C_{fbf}}} \tag{21}$$

For the case of constant values of τ_{bf}^*, C_{fbf}, R and D considered here, the implication is that flow velocity U_{bf} remains constant downstream.

The condition described by (21), i.e. flow velocity at bankfull flow that remains constant in the downstream direction, is approximate, and is only as good as the assumptions of constant friction coefficient C_{fbf} and Shields number τ_{bf}^* in (21). These caveats notwithstanding, a considerable body of evidence suggests that U_{bf} increases only slowly downstream, with values of m between 0 and 0.1 in the proportionality

$$U_{bf} \propto Q_{bf}^m \tag{22}$$

(e.g. Richards, 1982). In the present case of a stream reach without tributaries, it can be expected that the exponent m would be toward the lower end of this range.

For self-formed rivers, then, (16a) reduces with the aid of (2b), (11) and (21) to

$$\frac{dH_{bf}}{dx} = S - S_{fric} \quad , \quad S_{fric} = \frac{RD\tau^*_{form}}{H_{bf}} \qquad \text{(23a,b)}$$

That is, (23) provides an appropriate description of backwater in self-formed sand-bed streams. The boundary condition on (23a) is given by a form of (8a) applied at the topset-foreset break to bankfull flow. As outlined below, however, when backwater effects are included the position of the topset-foreset break, here denoted as $x = s_{tf}(t)$, can no longer be unambiguously identified with the shoreline position $x = s_s(t)$ used in the analysis of the experiments of Muto (2001). Thus (8a) becomes

$$H_{bf}[s_{tf}(t), t] = \xi(t) - \eta[s_{tf}(t), t] \qquad \text{(24)}$$

If at any time the sea level $\xi(t)$ and the bed profile $\eta(x,t)$ up to $x = s_{tf}(t)$ are known, the streamwise profile of bankfull depth $H_{bf}(x,t)$ can be computed from a solution of (23a) subject to (24)

A backwater formulation describes a mildly disequilibrium flow in a river. Here it is also assumed that the morphodynamics of the river itself is in mild disequilibrium as it responds to sea level rise. More precisely, it is assumed that as the river aggrades it has enough time to build a channel and floodplain so that the bankfull Shields number defined by friction slope can be maintained at a nearly constant channel-forming value close to 1.86, i.e.

$$\tau_{bf}^* = \frac{H_{bf} S_{fric}}{RD} = \tau_{form}^* \qquad (25)$$

This by no means implies that the channel is in grade, because in order to achieve a completely graded channel S_{fric} would need to be precisely equal to bed slope S (no backwater effects) and the local sand transport rate Q_{sbf} would have to be equal to the feed rate $Q_{sbff.}$

The quasi-equilibrium forms (12), (13) and (14) must be generalized as follows to include the case of non-negligible backwater effects. The constant flow velocity U_{bf} is calculated from (21). Consider a topset bed profile $\eta(x,t)$, $s_{ba}(t) \le x \le s_{tf}(t)$ that is known at any time t. Downchannel bed slope S is then calculated from this profile according to (2). Channel depth $H_{bf}(x,t)$ is computed at time t by integrating (23a) subject to (24). Channel width $B_{bf}(x,t)$ is then computed from (5) and the known values of Q_{bf}, U_{bf} and H_{bf}, i.e.

$$B_{bf} = \frac{Q_{bf}}{U_{bf} H_{bf}} \qquad (26)$$

Finally the sediment transport rate $Q_{sbf}(x,t)$ is computed from (9), which takes the dimensioned form

$$Q_{sbf} = B_{bf} \sqrt{RgD}\, D\, 0.05 Cz_{bf}^2 (\tau_{form}^*)^{2.5} \qquad (27)$$

It is easily verified that this formulation reduces to (12) – (14) in the event that backwater is neglected in (23).

The above formulation cannot be used all the way to the topset-foreset break during sediment-starved autoretreat driven by base level rise. This is because the topset-foreset break is abandoned during sediment-starved autoretreat, resulting in the formation of an embayment (Fig. 8). The embayment perforce drowns the river and renders channel-forming processes inoperative. Were a channel with constant Shields number τ^*_{form} applied through the embayment, the result would be an ever-narrower channel in ever-deeper water that would still be capable of transporting at least some sediment. This can be seen from (26) reduced with (21) and (25);

$$B_{bf} = \frac{\sqrt{C_{fbf}}\, Q_{bf}}{\sqrt{RgD}\, \tau^*_{form} H_{bf}} \tag{28}$$

Since all terms in (28) are approximated here as constants except flow depth H_{bf}, ever-increasing depth in the embayment would imply ever-decreasing bankfull width in a zone where channel construction has been turned off due to drowning (Fig. 8).

In order for the model to be physically realistic, then, it is necessary to abandon the assumption of a self-formed channel within the embayment. The existence of an embayment of essentially standing water can be recognized in terms of the ratio of the friction slope S_{fric} given by (23) to the bed slope S. When the condition

$$\frac{S_{fric}}{S} << 1 \tag{29}$$

is satisfied, (23) reduces with (2) to the approximate form

$$\eta + H_{bf} = \text{const in } x = \xi(t) \tag{30}$$

That is, the elevation of the water surface in the river valley becomes equal to that of the sea, implying drowning of the valley.

In the present analysis the channel floodplain width B_f (which is assumed to be consonant with the valley width) is taken to be a constant. Drowning during sediment-starved autoretreat can be reproduced in the model by generalizing (23), (26) and (27) to the forms

$$\begin{aligned} \frac{dH_{bf}}{dx} &= S - S_{fric} \quad , \quad S_{fric}/S \geq r_S \quad \text{(active channel present)} \\ H_{bf} &= \xi(t) - \eta(x,t) \quad , \quad S_{fric}/S < r_S \quad \text{(channel drowned)} \end{aligned} \qquad (31a,b)$$

$$B_{bf} = \begin{cases} \dfrac{Q_{bf}}{U_{bf}H_{bf}} \quad , \quad S_f/S \geq r_S \quad \text{(active channel present)} \\ B_f \quad , \quad S_f/S < r_S \quad \text{(channel drowned)} \end{cases} \qquad (32)$$

$$Q_{sbf} = \begin{cases} B_{bf}\sqrt{RgD}\,D\,0.05Cz_{bf}^2(\tau_{form}^*)^{2.5} \; , S_{fric}/S \geq r_S \quad \text{(active channel present)} \\ 0 \; , S_{fric}/S < r_S \quad \text{(channel drowned)} \end{cases}$$

(33)

where r_S is a suitable constant less than unity. In the calculations below this constant is set equal to 0.3. This value was determined by trial and error such that the shoreline was identified correctly when the river mouth underwent sediment-starved autoretreat.

The above adaptation of the model is illustrated in Fig. 8. During sediment-starved autoretreat the approximate position of the shoreline is equal to the point x where S_{fric}/S becomes equal to r_S, a point that can be well upstream of the abandoned topset-foreset break.

Floodplain construction and wash load The form of the Exner equation of sediment conservation (3) of Part I used to describe the experiments of Muto (2001) is too simple to describe the response of sand-bed rivers to aggradation over thousands of years. Here it is assumed that as the river bed aggrades, the river is eventually able to rework its floodplain by means of channel migration and avulsion.

Sediment in transport is typically divided into "bed material load," i.e. moving sediment of a size range that actively exchanges with the bed, and "wash load," i.e. moving sediment that is too fine to be contained in measurable quantities in the bed. Wash load is typically taken to be material finer than 62 μm, and is therefore material in the silt/clay size range (mud). In standard treatments of morphodynamics the wash load is ignored. Here, however, it is treated as "floodplain material load" that actively exchanges with the floodplain. That is, while the river bed is assumed to be composed solely of sand at any time, the process of migration and avulsion allows the deposition of considerable quantities of mud on the floodplain.

The volume sand (bed material) load at bankfull flow is denoted as before as Q_{sbf}, and the volume mud (floodplain material) load at bankfull flow is denoted as Q_{mbf}. The mean annual mass transport rates of sand M_{sand} and sediment (sand + mud) M_{sed} are thus given as

$$\begin{aligned} M_{sand} &= \rho_s I_f Q_{sbf} \\ M_{sed} &= \rho_s I_f (Q_{sbf} + Q_{mbf}) \end{aligned} \qquad (34a,b)$$

Denoting the feed rate of mud from upstream as Q_{mbff}, the mean annual feed rates of sand M_{sandf} and sediment (sand + mud) M_{sedf} to the reach to be modeled are

$$\begin{aligned} M_{sandf} &= \rho_s I_f Q_{sbff} \\ M_{sedf} &= \rho_s I_f (Q_{sbff} + Q_{mbff}) \end{aligned} \qquad (34c,d)$$

Consider the diagram of Fig. 9. The downchannel coordinate is x and the downvalley coordinate is x_v. Averaging over many meander bends, the relation between the two is

$$\frac{dx}{dx_v} = \Omega \tag{35}$$

where Ω denotes channel sinuosity, here taken to be constant. Sediment is transported in a channel of width B_{bf}, but in the long term is deposited over a much wider floodplain with width B_f, here taken to be constant. Thus sediment conservation for the reach in question is

$$\frac{\partial}{\partial t}\rho_s B_f (1-\lambda_p)\eta \Delta x_v = \rho_s I_f \left(Q_{sbf} + Q_{mbf}\right)\Big|_x - \rho_s I_f \left(Q_{sbf} + Q_{mbf}\right)\Big|_{x+\Delta x} \tag{36}$$

where λ_p denotes the mean porosity of the channel-floodplain complex. Reducing (36) with (35), then,

$$(1-\lambda_p)\frac{\partial \eta}{\partial t} = -\Omega \frac{I_f}{B_f}\left(\frac{\partial Q_{sbf}}{\partial x} + \frac{\partial Q_{mbf}}{\partial x}\right) \tag{37}$$

The process of floodplain deposition is not particularly well understood. With this in mind, the problem is simplified as follows. For every unit of sand deposited in the channel-floodplain complex, it is assumed that Λ units of mud are deposited. That is,

$$\frac{\partial Q_{mbf}}{\partial x} = \Lambda \frac{\partial Q_{sbf}}{\partial x} \tag{38}$$

where here Λ is approximated as a constant. The value of Λ can be estimated by means of an analysis of deposits in channel-floodplain complexes (e.g.

Törnqvist, 1993). Between (37) and (38), then, the final form of the Exner equation of sediment conservation for the long-term evolution of an aggrading sand-bed river is obtained:

$$(1-\lambda_p)\frac{\partial \eta}{\partial t} = -(1+\Lambda)\Omega\frac{I_f}{B_f}\frac{\partial Q_{sbf}}{\partial x} \tag{39}$$

Differentiation between subaerial and subaqueous basement profiles In the experiments of Muto (2001) the model bedrock basement had a spatially constant slope S_b in each experiment. Thus the subaerial bedrock-alluvial transition and the foreset-subaqueous basement transition occurred on a basement of the same slope. In the case of rivers, however, the subaerial bedrock slope near the bedrock-alluvial transition can differ from that of the subaqueous basement over which the delta progrades. In order to represent this in a simple way, the basement slope at the bedrock-alluvial transition is denoted as S_{bb} and the basement slope at the foreset-subaqueous basement transition is denoted as S_{sb}, as illustrated in Fig. 10. That is,

$$S_{bb} = -\left.\frac{\partial \eta_{base}}{\partial x}\right|_{s_{ba}} \quad , \quad S_{sb} = -\left.\frac{\partial \eta_{base}}{\partial x}\right|_{s_{sb}} \tag{40a,b}$$

Both are kept constant in any given numerical run, but they need not be equal.

Decoupling of shoreline water surface elevation and topset-foreset break elevation In the experiments of Muto (2001), as long as the river delta was not in sediment-starved autoretreat it was possible to equate the elevation of the topset-foreset break with that of the water surface there. In large rivers with significant backwater effects, however, the depth H is sufficiently large to render this approximation inaccurate. The condition (8a) may thus be rephrased for bankfull flow as (24), according to which the difference between sea level and the bed elevation at the topset-foreset break is equal to the river depth at the topset-foreset break.

Condition (8c) must then be replaced with the following relation obtained from the chain rule. Recalling that the position of the topset-foreset break is denoted as $x = s_{tf}(t)$,

$$\frac{d}{dt}\eta[s_{tf}(t),t] = \left.\frac{\partial\eta}{\partial t}\right|_{s_{tf}} - S_{ttf}\dot{s} \quad , \quad S_{ttf} = -\left.\frac{\partial\eta}{\partial x}\right|_{s_{tf,topset}} \qquad \text{(41a,b)}$$

where S_{ttf} specifically denotes the topset slope at the topset-foreset transition. A comparison of (8c) and (41) clearly reveals that the elevation of the topset-foreset break has been decoupled from that of the water surface above it in the latter relation. The continuity condition (11) still holds at the foreset-subaqueous basement break; taking the derivative with respect to time and reducing with (37a) instead of (8c) results in:

$$\dot{s}_{sb} = \frac{S_{fore} - S_{ttf}}{S_{fore} - S_{sb}}\dot{s}_{tf} + \frac{1}{S_{fore} - S_{sb}}\left.\frac{\partial\eta}{\partial t}\right|_{s_{tf}} \qquad \text{(42)}$$

The shock condition across the foreset is obtained by integrating (39) from s_s to s_{sb} under the condition of vanishing load at the foreset-subaqueous basement break. It is assumed here that only sand deposits on the foreset, with the mud delivered to the shoreline dispersed in a negligibly thin layer over a wide area of sea floor. This allows the approximation of Λ as 0 across the foreset. Differentiating (9) with respect to time and reducing with (41) yields the following form for $\partial\eta/\partial t$ on the foreset:

$$\frac{\partial \eta}{\partial t} = \left.\frac{\partial \eta}{\partial t}\right|_{s_{tf}} + (S_{fore} - S_{ttf})\dot{s}_{tf} \tag{43}$$

Integrating (39) from s_s to s_{sb} and reducing the result with (43) and the condition of vanishing load at the foreset-subaqueous basement break results in the following shock condition:

$$(1-\lambda_p)B_f(s_{sb} - s_{tf})\left[(S_{fore} - S_{ttf})\dot{s}_{tf} + \left.\frac{\partial \eta}{\partial t}\right|_{x=s_{tf}}\right] = I_f Q_{sbf}\Big|_{x=s_{tf}} \tag{44}$$

The above relation describes the shock condition applied when the delta is not in sediment-starved autoretreat. The case of sediment-starved autoretreat is described by a shoreline located at the position where

$$S_{fric} = r_S S \tag{45}$$

as described above.

NUMERICAL FORMULATION AND IMPLEMENTATION: FIELD SCALE

Initial conditions The initial conditions represent a modest adaptation of those used to model the experiments of Muto (2001). As in the case of those experiments, s_{ba} is initially set equal to 0, s_{tf} is initially set equal to s_{tfi} and the initial downchannel fluvial bed slope to S_{fi}. Because the elevation of the topset-foreset break and sea level has been decoupled, however, it is necessary to specify the initial values of these two separately;

$$\eta[s_{tfi}, 0] = \eta_{ti} \quad , \quad \xi(0) = \xi_i \tag{46a,b}$$

where $\xi_i > \eta[s_{tfi}, 0]$. Where s_{sbi} denotes the initial value of s_{sb}, the initial elevation of the foreset-subaqueous basement break is given as

$$\eta[s_{sbi},0] = \eta_{bi} \tag{47}$$

The relation between s_{si}, s_{sbi} η_{ti} and η_{bi} is seen from Fig. 8a of Part I to be

$$s_{sbi} = s_{tfi} + \frac{\eta_{ti} - \eta_{bi}}{S_{fore}} \tag{48}$$

Transformation to moving boundary coordinates The moving boundary coordinates are identical to those used in the modeling of the experiments of Muto (2001) with the exception of the transformation $s_s \to s_{tf}$. In analogy to (22) of Part I (Parker *et al.*, submitted), the Exner equation of sediment continuity (39) transforms to

$$\frac{\partial \eta}{\partial \bar{t}} - \frac{[\bar{x}\dot{s}_{tf} + (1-\bar{x})\dot{s}_{ba}]}{s_{tf} - s_{ba}} \frac{\partial \eta}{\partial \bar{x}} = -\frac{I_f \Omega (1+\Lambda)}{B_f (1-\lambda_p)(s_{tf} - s_{ba})} \frac{\partial Q_{sbf}}{\partial \bar{x}} \tag{49}$$

The analog of (23) of Part I is the upstream boundary condition

$$Q_{sbf}\big|_{\bar{x}=0} = Q_{sbff} \tag{50}$$

The analog of (24) of Part I is the following condition for the migration speed of the bedrock-alluvial transition:

$$\dot{s}_{ba} = -\frac{1}{S_{bb}} \frac{\partial \eta}{\partial \bar{t}}\bigg|_{\bar{x}=0} \tag{51}$$

No analog to (25) of Part I is used in the application to rivers, because sea level and topset-foreset break elevation have been decoupled from each other. The analogs of (26) and (27) of Part I are, respectively,

$$\dot{s}_{sb} = \frac{1}{S_{fore} - S_{sb}} \left(S_{fore}\dot{s}_{tf} + \frac{\partial \eta}{\partial \bar{t}}\bigg|_{\bar{x}=1} \right) \tag{52}$$

$$\dot{s}_{tf} = \frac{1}{S_{fore}} \left[\frac{I_f \Omega}{(1-\lambda_p) B_f (s_{sb} - s_{tf})} Q_{sbf}\big|_{\bar{x}=1} - \frac{\partial \eta}{\partial \bar{t}}\bigg|_{\bar{x}=1} \right] \tag{53}$$

A comparison of (49) to (22) of Part I, (50) to (23) of Part I, (51) to (24) of Part I, (52) to (26) of Part I and (53) to (27) of Part I reveals that the model applied to the experiments of Muto (2001) and the model adapted for rivers are subsets of a unified structure. In the application to rivers, the inclusion of backwater effects results in the following forms for (31a,b) and (24) in moving boundary coordinates:

$$\frac{dH_{bf}}{d\bar{x}} = (s_{tf} - s_{ba})(S - S_{fric}) \quad , \quad S_{fric}/S \geq r_S$$
$$H_{bf} = \xi(\bar{t}) - \eta(\bar{x},\bar{t}) \quad , \quad S_{fric}/S < r_S \qquad (54a,b)$$

$$H_{bf}\big|_{\bar{x}=1} = \xi(\bar{t}) - \eta(1,\bar{t}) \qquad (55)$$

where S_{fric} is given by (23b)

Discretization and flow of the calculation As before, the alluvial domain $0 \leq \bar{x} \leq 1$ is discretized into N intervals, each with length Δx given by (30), bounded by N+1 nodes i = 1..N+1. Let the bed profile $\eta(\bar{x}, t)$ (discretized to η_i) be given at any time. The flow depths $H_{bf,i}$ are then computed everywhere from an upstream integration of (54) subject to (55). In the case of (54a), this is carried out using a predictor-corrector method; proceeding upstream from either i = N+1 or the farthest downstream node for which the condition $S_{fric}/S \geq r_S$ is satisfied to i = 2,

$$H_{bf,pred} = H_{bf,i} + (s_{tf} - s_{ba})\left[(\eta_i - \eta_{i-1}) - \frac{RD\tau^*_{form}}{H_{bf,i}}\Delta\bar{x}\right] \qquad (56a)$$

$$H_{bf,i-1} = H_{bf,i} + \frac{1}{2}(s_{tf} - s_{ba})\left\{\left[(\eta_i - \eta_{i-1}) - \frac{RD\tau^*_{form}}{H_{bf,i}}\Delta\bar{x}\right] + \left[(\eta_i - \eta_{i-1}) - \frac{RD\tau^*_{form}}{H_{bf,pred}}\Delta\bar{x}\right]\right\}$$

(56b)

Channel width $B_{bf,i}$ is computed everywhere from (32) and the sand transport rate $Q_{sbf,i}$ is computed everywhere from (33). The migration speeds $\dot{s}_{ba}$, $\dot{s}_{tf}$ and $\dot{s}_{sb}$ are computed from (51), (53) and (52) respectively. Once Q_{sbf}, $\dot{s}_{ba}$, $\dot{s}_{tf}$ and $\dot{s}_{sb}$ are known the bed elevation profile at time $\Delta\bar{t}$ later is computed from a discretized version of (49);

$$\eta_i\Big|_{\bar{t}+\Delta\bar{t}} = \eta_i + \frac{[\bar{x}_i\dot{s}_{tf} + (1-\bar{x}_i)\dot{s}_{ba}]}{s_{tf} - s_{ba}}\frac{\partial\eta}{\partial\bar{x}}\bigg|_i \Delta\bar{t} - \frac{I_f\Omega(1+\Lambda)}{B_f(1-\lambda_p)(s_{tf}-s_{ba})}\frac{\partial Q_{sbf}}{\partial\bar{x}}\bigg|_i \Delta\bar{t} \tag{57}$$

where η_i denotes the bed elevation at the ith node at time $\bar{t}$, and the indicated derivates are computed as follows:

$$\frac{\partial\eta}{\partial\bar{x}}\bigg|_i = \begin{cases} \dfrac{\eta_{i+1}-\eta_i}{\Delta\bar{x}} & , \quad i = 1..N \\[2ex] \dfrac{\eta_i - \eta_{i-1}}{\Delta\bar{x}} & , \quad i = N+1 \end{cases} \tag{58a,b}$$

$$\frac{\partial Q_{sbf}}{\partial\bar{x}}\bigg|_i = \begin{cases} \dfrac{Q_{sbf,i}-Q_{sbff}}{\Delta\bar{x}} & , \quad i = 1 \\[2ex] \dfrac{Q_{sbf,i} - Q_{sbf,i-1}}{\Delta x} & , \quad i = 2..N+1 \end{cases} \tag{59a,b}$$

Relations (51), (52), (53) and (57) are implicit, in that a knowledge of $\partial\eta/\partial\bar{t}$ at $\bar{x}=0$ and $\bar{x}=1$ is required in order to compute $\dot{s}_{ba}$, $\dot{s}_{tf}$ and $\dot{s}_{sb}$, but a knowledge of $\dot{s}_{ba}$, $\dot{s}_{tf}$ and $\dot{s}_{sb}$ is required to compute $\partial\eta/\partial\bar{t}$, and thus η at $\bar{t}+\Delta\bar{t}$. The relations can be made explicit by adding two compatibility relations obtained by evaluating (49) at $\bar{x}=0$ and $\bar{x}=1$;

$$\frac{\partial\eta}{\partial\bar{t}}\bigg|_{\bar{x}=0} = \frac{\dot{s}_{ba}}{s_{tf}-s_{ba}}\frac{\partial\eta}{\partial\bar{x}}\bigg|_{\bar{x}=0} - \frac{I_f\Omega(1+\Lambda)}{B_f(1-\lambda_p)(s_{tf}-s_{ba})}\frac{\partial Q_{sbf}}{\partial\bar{x}}\bigg|_{\bar{x}=0} \tag{60}$$

$$\left.\frac{\partial\eta}{\partial\bar{t}}\right|_{\bar{x}=1} = \frac{\dot{s}_{tf}}{s_{tf}-s_{ba}}\left.\frac{\partial\eta}{\partial\bar{x}}\right|_{\bar{x}=1} - \frac{I_f\Omega(1+\Lambda)}{B_f(1-\lambda_p)(s_{tf}-s_{ba})}\left.\frac{\partial Q_{sbf}}{\partial\bar{x}}\right|_{\bar{x}=1} \tag{61}$$

Treatment of sediment-starved autoretreat, and recommencement of delta progradation after the cessation of sea level rise The analog of (28) describing a sediment-starved shoreline is (45). In principle, when the river delta goes into sediment-starved autoretreat the transformation $s_{tf} \rightarrow s_s$ should be made in equations (49), (52), (53), (54), (56), (57), (60) and (61), where the position of the shoreline s_s is found iteratively from the relation

$$\left.\frac{S_f}{S}\right|_{\bar{x}=s_s} = r_S \tag{62}$$

While the position of the shoreline during sediment-starved autoretreat is tracked in the implementation below, the transformation $s_{tf} \rightarrow s_s$ is not made in the formulation for two reasons. The first is because little error appears to result over the conditions studied. The second relates to the cessation of sediment-starved autoretreat upon the stabilization of sea level. Preservation of the entire mesh from $\bar{x} = 0$ to $\bar{x} = s_{tf}$ in memory (without truncation at the shoreline) allows for a resumption of delta progradation over the antecedent bed without regridding and interpolating. When delta progradation resumes, the delta is located by means of shock-capturing rather than the shock-fitting technique of (53). The abandoned topset-foreset break is reactivated, and (53) re-implemented, when the shock-captured delta progrades beyond the delta abandoned by sediment-starved autoretreat.

QUANTIFICATION OF THE FLY-STRICKLAND RIVER SYSTEM

As noted above, it is crudely assumed here that both local hydrologic regime and sediment supply have not been greatly altered in the Fly-Strickland River system from the last glacial maximum to the present. As a result, in the present analysis it is assumed that the effect of global climate change on the sand-bed Fly-Strickland River System is driven solely by 120 m of eustatic sea level rise. As also noted above, the sand-bed system is abstracted to a single sand-bed stream with no tributaries.

The Strickland River from the gravel-sand transition to Everill Junction has a channel sinuosity Ω of about 2.25 and a floodplain width B_f of 8000 m; from Everill Junction to the end of the fluvial reach (EFF in Fig. 1) the corresponding values are 1.6 and 15000 m. For simplicity the two reaches are lumped together here as a single reach with a constant sinuosity Ω of 2.0 and a constant floodplain width B_f of 12000 m. It is reasonable to assume that at low stand the river extended to a point near the present shelf-slope break. Using the adjusted sinuosity of 2.0, the following downchannel distances are estimated.

- Present-day gravel-sand transition to Everill Junction: 240 km.
- Everill Junction to end of fluvial reach (EFR of Fig. 1): 240 km.
- EFR to beginning of the estuary flare (BEF of Fig. 1): 200 km.
- BEF to outer edge of the estuary (OEE of Fig. 1): 160 km.
- OEE to shelf-slope break: 290 km.

Thus the adjusted downchannel distance from the present-day gravel-sand transition to the present-day shelf-slope break is estimated to be 1130 km. Note that the downchannel distance from Everill Junction to the gravel-sand transition given above, i.e. 240 km, differs from the actual value of 269 km given in the section "THE FLY-STRICKLAND RIVER SYSTEM, PAPUA NEW GUINEA," because the value of 240 km is based on an overall bulk sinuosity for the entire Strickland River of 2.0 rather than the actual value of 2.25 over the reach in question.

The mean annual discharges of the Strickland and Fly Rivers at Everill Junction were previously quoted as 3100 m^3/s and 2240 m^3/s. Recalling that bankfull discharges in the sand-bed Fly-Strickland River system are only modestly above mean annual values, a single bankfull discharge Q_{bf} of 5700 m^3/s is selected to model a single reach with no tributaries from the gravel-sand transition of the Strickland River to the mouth. A relatively high flood intermittency I_f of 0.175 is selected to reflect the relative frequency of overbank events. Hydrologic measurements on the Strickland River are not of sufficient detail to verify this number. The number is, however, in the measured range for the Fly River near D'Albertis Junction (Fig. 1), a reach with similar characteristics to the Strickland River, i.e. S ~ 0.00005 (about half of the Strickland River at Everill Junction) and D ~ 0.25 mm (about the same as the Strickland River at Everill Junction (Cui and Parker, 1999). A single sediment size D of 0.25 mm is selected for this reach based on measurements by Ok Tedi Mining Ltd. at Ogwa, a bar just below Everill Junction. Sediment specific gravity is assumed to be 2.65, so that R = 1.65.

The present-day slope of the Strickland River from the gravel-sand transition to Everill Junction is about 0.00010. The slope of the gravel-bed reach immediately upstream of the gravel-sand transition is near 0.00046; this value is here treated as the slope S_{bb} of a bedrock reach immediately upstream of the gravel-sand transition. Relations (12) – (14) were used in conjunction with (8) and (10) to estimate the bankfull sand feed rate Q_{sbff}, bankfull Chezy resistance coefficient Cz_{bf} and channel-forming Shields number τ^*_{form} at the upstream end of the reach assuming a measured bankfull width B_{bf} of 350 m, an estimated bankfull depth H_{bf} of 7.5 m and a measured bed slope S of 0.0001; these values were found to be Q_{sbff} = 0.795 m^3/s, Cz_{bf} = 25.3 and τ^*_{form} = 1.818.

In light of the uncertainties of the above calculation, Q_{sbff}, Cz_{bf} and τ^*_{form} are rounded to 0.80, 25 and 1.82, respectively. Recalculating from (12) and (14) results in the amended estimates for H_{bf}, B_{bf}, and S of 7.38 m, 360 m and 0.00102, respectively; the corresponding Froude number $\mathbf{Fr}_{bf}$ is 0.252. The estimates for Cz_{bf}, τ^*_{form} and $\mathbf{Fr}_{bf}$ obtained in this way are plotted with other data for sand-bed and gravel-bed streams in Figs. 5, 6 and 7. These estimates for the Strickland River fall comfortably within the scatter of the values for other sand-bed rivers. The value of Q_{sbff} of 0.80 m^3/s combined with the above-quoted value of I_f and reasonable assumption that 15% of the load of the Strickland River is sand yields a mean annual sediment feed rate M_{sedf} (sand and mud) of 78.1 Mt/a, a value that is very close to the sum of the previously-quoted loads for the Strickland and Fly Rivers at Everill Junction of 70 Mt/a and 8 Mt/a, respectively.

The calculation begins at low stand, when the river extends to the shelf-slope break. Using present-day sea level as a datum, elevation of the topset-foreset break η_{ti} at the beginning of the calculation is set to – 130 m under the assumption of a channel with a bankfull depth of 10 m and a bank elevation of – 120 m. Based on available field bathymetry, the initial elevation of the foreset-subaqueous basement break η_{bi} is set equal to – 170 m. The distance from the topset-foreset break to the foreset-subaqueous basement break is 25 km, so that S_{fore} becomes 0.0016 (0.092°). The slope S_{bs} of the subaqueous basement, i.e. the continental shelf, was found to be near 0.00075 (0.043°).

In the absence of other guiding information, the initial fluvial bed slope S_{fi} at the glacial maximum is set equal to the value 0.0001 estimated to be near the equilibrium (graded) slope of the sand-bed stream at the present-day gravel-sand transition. Since the distance from Everill Junction to the shelf edge is estimated to be 890 km, the implication is an initial elevation at Everill Junction of – 41 m.

The porosity λ_p of the deposit in the channel-floodplain complex is estimated as 0.35, a value that is intended to account for the effect of compaction over thousands of years. Perhaps the hardest parameter to estimate accurately is Λ, i.e. the ratio of mud deposited per unit sand. The boreholes and seismic surveys necessary to estimate this parameter are not available for the Fly-Strickland River system. Here Λ is crudely set equal to unity based on information pertaining to the Rhine River (Törnqvist, personal communication in 2003).

The input parameters outlined above are summarized in Table 1.

MODELING SCENARIOS

Three cases are considered in the calculations of the next section. All three begin at - 21000 years relative to the present (21000 years BP). Case A is a reference case for which sea level is held constant at – 120 m for 21000 years. In Case B, sea level is constant at – 120 m for the first 3000 years, rises at 10 mm/year for 12000 years to an elevation of 0 m, and is subsequently constant for 6000 years; the total simulated time is again 21000 years. As shown in Fig. 1, Case B thus provides a reasonably approximation of Pleistocene-Holocene sea level rise as described by the curve of Fig. 1 of Part I due to Bard et al. (1996). Case C is identical to Case B except that a) the sand feed rate Q_{sbff} is increased by a factor of 2.92 from 0.80 m^3/s to 2.336 m^3/s, and b) the initial fluvial bed slope S_{fi} is increased by the same factor. The increase in S_{fi} along with Q_{sbff}, while not necessary for the calculations, ensures comparability of the results. This is because the parameters for Case B were determined by assuming from the use of e.g. (15) and the assumption of an initial channel that is in grade. According to (14), the slope S (initial value S_{fi} in this case) increases linearly with bankfull sand discharge Q_{sbf} (feed value Q_{sbff} in this case) in a graded channel in which all other parameters are held constant.

The initial length of the fluvial reach s_{tfi} must be close to the present downchannel distance from the gravel-sand transition to the shelf edge, here estimated as 1130 km. A value of s_{tfi} of 970 km was found to reproduce this distance under the conditions of Case B outlined above. This value is thus adopted for all calculations given below.

Case A addresses the following scenario: what if Pleistocene-Holocene sea level rise never occurred, and instead sea level remained constant at its value corresponding to the glacial maximum from – 21000 years until 0 years (present)? Case B addresses a scenario that is reasonably close to what actually occurred, i.e. 3000 years at minimum stand, 12000 years of sea level rise at 10 mm/year, and then 6000 years at the present high stand. As outlined below, the calculation indicates that the Fly River mouth goes into sediment-starved autoretreat, and moves some 768 km upstream of the abandoned delta, before forming a new delta and resuming progradation.

Case C addresses the following query: is there a sediment feed rate sufficiently high to prevent the Strickland River from going into sediment-starved autoretreat throughout the 120 m of Pleistocene-Holocene sea level rise? In performing the calculations, Q_{sbff} and S_{fi} were both increased by the multiplicative factor Q_{srat}, leaving all other parameters the same as Case B, and the lowest value of Q_{srat} for which the shoreline never abandons the delta was sought. This was found to be Q_{srat} = 2.92, or Q_{sbff} = 2.336 m^3/s (as compared to 0.80 m^3/s for Case B).

In the calculations for the three cases below the number of spatial intervals N has been set equal to 135 and the time step $\Delta\bar{t}$ has been set equal to 1.5 years.

MODELING RESULTS

Throughout this section reference is made to a “gravel-sand transition.” It should be borne in mind, however, that in the model this transition is approximated as a bedrock-alluvial transition.

Case A Results for Case A are summarized in Figs. 11a-e. Fig. 11a shows the bed profiles for the eight times t = -21000 years, - 18000 years, - 15000 years, -12000 years, - 9000 years, - 6000 years, -3000 years and 0 years (present), as well as the water surface profile at 0 years (present). The river delta monotonically progrades outward (shoreline regresses) the whole time. The profiles appear to have an almost constant slope. In fact the profiles are upward concave, with a slope that decreases downstream, but the decrease is slight. By 0 years (present) the bed slope decreases from 0.000103 at the gravel-sand transition to 0.0000921 at the topset-foreset break some 1086 km downstream, i.e. a decrease of only 10.4%.

Part of the reason for the slight upward concavity is due to the fact that the delta progrades onto a subaqueous basement (continental shelf) that has a slope some 7 ~ 8 times higher than ambient river slopes. When the same calculation is performed on a horizontal subaqueous basement, the corresponding downstream decrease in slope is 20.9%.

Figures 11b and 11c show the streamwise variation in bankfull river width B_{bf} and volume sand transport rate at bankfull flow Q_{sbf} at the same eight times as above, i.e. t = -21000 years, - 18000 years, -15000 years, -12000 years, - 9000 years, - 6000 years, -3000 years and 0 years (present). These two parameters track each other in accordance with (13). The slight upward concavity of Fig. 11a implies that the sand transport rate slightly declines downstream as sediment deposits in the channel/floodplain complex. As a result, Q_{sbf} decreases only slightly downstream. Since at the same bankfull discharge Q_{bf} a lower value of Q_{sbf} can be transported by a narrower channel in accordance with (13), B_{bf} also decreases slightly downstream. For practical purposes, however both parameters are nearly constant downstream by – 18000 years, and remain so until the present. Note that all the lines after t = - 21000 years approximately collapse together in a self-similar form, with the profile simply elongating in time as the delta progrades.

Figure 11d shows the corresponding streamwise variation in bankfull depth H_{bf}. Note that the depth strongly increases near the downstream end of the reach at the initial time t = - 21000 years. This is because the initial bed profile, which has absolutely no concavity (S_{fi} = 0.0001 everywhere), must first develop a weak upward concavity before it can prograde outward in an approximately self-similar form. By – 18000 years, however, such an approximate form is reached, and all subsequent curves plot roughly on top of each other.

Fig. 11e shows the position of the topset-foreset break $s_{tf}(t)$ along with the position of the shoreline $s_s(t)$ as identified by (62). The two are always equal to each other, and the delta is seen to prograde outward at an ever-decreasing rate. This is because as the delta progrades more and more sediment must be deposited on the elongating topset, leaving ever less to deposit on the foreset.

Over 21000 years the gravel-sand transition migrates upstream 19.7 km, and the river bed aggrades some 7.02 m above the elevation at the initial gravel-sand transition. The topset-foreset break progrades out 96.1 km over the same period. By t = 0 (present), the sand load Q_{sbf} declines modestly downstream from 0.80 m^3/s to 0.723 m^3/s, and bankfull width B_{bf} correspondingly declines modestly from 360 m to 326 m. Bankfull depth H_{bf} correspondingly increases modestly from 7.39 m to 8.16 m.

Case B Results for Case B are summarized in Figs. 12a-g. The formats of the first five of these figures are the same as Figs. 11a-e. Fig. 12a shows eight bed profiles, including the final one at t = 0 (present), along with the final water surface. The effect of 120 m of sea level rise between t = - 18000 years and t = - 6000 years is dramatic. The delta progrades outward for the first 3000 years of constant low stand. As sea level rise commences, the progradation rate declines, and eventually the original delta is abandoned and shoreline begins to transgress. The details of this transgression are elaborated below. It suffices to mention here that the shoreline transgresses well over 700 km by the time sea level stabilizes at high stand at t = - 6000 years. A new delta then forms and progrades outward to its final position at t = 0 (present).

Figs. 12b-c illustrate the variation in B_{bf} and Q_{sbf} under the conditions of Case B. The sudden increase B_{bf} to the valley width B_f of 12000 m in Fig. 25b tracks the point at which the river mouth is drowned, which is also where the sand transport rate drops to zero in Fig. 25c. It is thus seen in the figures that the river mouth undergoes sediment-starved autoretreat between about t = -

18000 years and about t = - 6000 years, and then forms a new delta and progrades outward.

The notable downstream decreases in sand load in Fig. 12c and corresponding decrease in bankfull width in Fig. 12b during autoretreat are clearly reflected in the bed elevation profiles of Fig. 12a. Autoretreat forces a high rate of sediment deposition and consequent bed aggradation that propagates well upstream of the shoreline. The result is a gravel-sand transition that propagates some 134.5 km upstream over 21000 years as sand onlaps onto the steeper slope. This value compares with only 19.7 km in Case A. Similarly, in Case B the river bed aggrades 48.0 m above the elevation at the initial gravel-sand transition; in Case A the corresponding value was only 7.0 m.

Lake Murray, shown in Figs. 1 and 2, is the largest blocked-valley lake on the Fly-Strickland River system. The Herbert River connects Lake Murray to the Strickland River; it joins the Strickland River between Everill Junction and the gravel-sand transition. The predicted riverbed aggradation of ~ 50 m in this reach seen in Fig. 25a would have been more than sufficient to create Lake Murray.

The downstream decreases in B_{bf} and Q_{sbf} in Figs. 12b-c corresponding to a pattern of bankfull depth H_{bf} that increases strongly in the downstream direction during autoretreat, as seen in Fig. 12d. This strong increase documents the gradual drowning of the river valley by the encroaching sea. The downstream increase in H_{bf} and decreases in B_{bf} and Q_{sbf} are seen to be ameliorated after t =

- 6000 years, when sea level rise stops and a new delta begins to prograde outward.

Fig. 12e documents the distance from the original position of the gravel-sand transition to a) the topset-foreset break of the original delta and b) the shoreline for Case B. The initial delta is abandoned by about t = - 15000 years and the river mouth goes into autoretreat until sea level rise stops at t = - 6000 years. After this time a new delta forms and progrades outward, forcing shoreline regression. Autoretreat causes the river mouth to step back some 767 km by end of sea level rise (t = - 6000 years). The new delta then progrades outward another 140.3 km, ending up 627.4 km upstream of initial position of delta.

Fig. 12f provides an expanded view of Fig. 12e that documents the details of autoretreat. The original delta is able to prograde outward from t = - 21000 years to t = - 15750 years, in spite of the fact that sea level rise starts at t = - 18000 years. From t = - 15750 years to t = - 14175 years the delta slowly backsteps in autoretreat without sediment starvation. Autobreak is reached at about t = - 14175 years, after which the river mouth retreats rapidly upstream under conditions of sediment starvation. While the details differ, the picture painted by the results of the numerical model is identical to that seen in Figs. 4 and 5 of the experiments of Muto (2001).

Fig. 12g provides a partial check on the model results. The plot shows profiles of the Strickland River upstream of Everill Junction. The small gray squares denote SRTM (Shuttle Radar Topographic Mission) data on river bank elevations. The solid diamonds denote bankfull water surface elevation computed at t = 0 (present) for Case B. (Computed distances have been adjusted so that the downchannel distance from the gravel-sand transition is the actual value of 269 km, not the nominal value of 240 km used in the model. This reflects the fact that the bulk channel sinuosity of the lumped Strickland River system was taken to be 2.0, whereas the channel sinuosity between Everill Junction and the gravel-sand transition is 2.25, as outlined in the section "QUANTIFICATION OF THE FLY-STRICKLAND RIVER SYSTEM").

The agreement between the measured profile and the computed profile for Case B at t = 0 (present), while not perfect, is remarkably good in so far as no attempt was made to match the profiles. The model uses a first assumption as to what the river profile must have been like at the last glacial maximum, i.e. a bed profile with a nearly constant slope ~ 0.0001 extending upstream from an elevation of – 130 m at the shelf edge. When subjected to the approximate sea level curve of the dashed line of Fig. 1 of Part I, the computed river profile between Everill Junction and the gravel-sand transition is in fact close to what is observed. The average computed water surface slope in Fig. 25g is 0.000078, or about 78% of the observed value. It is remarkable that this value is as close as it is to the observed value, in that parameters dependent on local climate such as Q_{bf}, I_f Q_{sbff} and D have been held constant throughout 21000 years.

One other point of interest can be seen by comparing Figs. 1 and 12a. Both figures contain the notation "EFR" denoting "end of the fluvial reach." As seen in Fig. 1, downstream of this point the river merges into a much-wider estuary. It is seen from Fig. 14a that the predicted present position of the delta that reforms after the end of sea level rise is not far from the end of the fluvial reach.

The modeling thus suggests that the end of the fluvial reach in Fig. 11 denotes the present-day position of a prograding delta, downstream of which is a tidal-dominated estuary. That is, the present-day estuary of the Fly River between points EFR and OEE ("outer edge of estuary") in Fig. 1 may be in part a consequence of autoretreat due to Pleistocene-Holocene sea level rise. The Fly River may be prograding outward into the Fly Estuary, constructing a fluvial channel as it does so, as it recovers from sea level rise.

The delta in Fig. 12a at t = 0 (present) has a foreset height of 33.4 m. No such high delta face is in fact observed near point EFR in Fig, 14. One reason for this may be that the modern Fly Estuary is subject to a notable tidal influence which has not been included in the model. The effect of cycled tides would be to smear out the foreset and pull sand well into the estuary. Perhaps more importantly, mud that reaches the topset-foreset break is not allowed to deposit to form an estuarine bottomset in the present simplified model. The deposition of mud would act to reduce the height of any delta. Kostic and Parker (2003a,b) and Swenson *et al.* (2005) provide numerical models which include bottomset or prodelta deposition.

Case C As illustrated by Muto (2001), all river mouths would go into autoretreat if sea level rise were sustained for a sufficiently long time. In the case of the Earth, however, the total amount and duration of sea level rise is controlled by the total amount of ice sequestered in glaciers at the glacial maximum. As a result, sea level rise cannot be sustained indefinitely.

All other factors being constant, an increase in sediment supply should act to delay the onset of autoretreat. If autoretreat is delayed beyond the time of cessation of sea level rise, a river delta may not be drowned at all. Even if the river does go into sediment-starved autoretreat, a river with a higher sediment load can be expected to recover faster. This factor may help explain the difference between the estuaries of Fig. 2 and the delta of Fig. 3, both of Part I.

Numerical experiments were performed to explore this issue. In particular, the sediment feed rate Q_{sbff} and initial fluvial slope S_{fi} were both increased by the same multiplicative factor Q_{srat}, keeping all other parameters constant, until a delta that barely fails to go into sediment-starved autoretreat was obtained. The critical value of Q_{srat} was found to be 2.92, corresponding to the values Q_{sbff} = 2.336 m^3/s and S_{fi} = 0.000292. These values were used for Case C, which is identical to Case B in all other respects.

The results for Case C are documented in Figs. 13a-e. It is seen in Fig. 13a that the delta does go into autoretreat without sediment starvation for a period, the shoreline never abandons the delta. The gravel-sand transition migrates upstream some 137 km in the course of the run, a value that is higher than the 134.5 km observed in Case B. This is because the much larger sediment load of Case C yields a much larger value of the alluvial slope S_{aba} at the transition, thus increasing the rate of onlapping in accordance with (7a). Only 24.4 m of aggradation, however, occurs at the original position of the gravel-sand transition, as compared to a value of 48 m computed for Case B. It can be seen from a comparison of Figs. 12a and 13a the absence of sediment-starved autoretreat in Case C has greatly reduced the upstream propagation of riverbed aggradation driven by sea level rise as compared to Case B, even though the sediment supply rate is nearly three times higher in Case C.

Figs. 13b-d document the changes in B_{bf}, Q_{bf} and H_{bf} computed for Case C. All three figures document a minor drowning of the delta at t = - 21000 years, i.e. the beginning of the run. This is because the profile has not yet reached an approximately self-similar state associated with progradation at constant sea level (as documented for Case A). This state is, however, achieved by t = -18,000 years, at which time the delta is actively prograding outward. Sea level rise commences at t = - 18000 years and ends at – 6000 years, as in Case B, but the river mouth is never drowned and the delta is never abandoned.

The fact that in Case C the shoreline never abandons the delta is documented in Fig. 13e. The delta undergoes mild autoretreat without sediment starvation from – 16500 years (1500 years after the start of sea level rise) – 3750 years (2250 years after the cessation of sea level rise).

Parametric study of the effect of increasing sediment load The effect of increasing sediment supply on river response to sea level rise is studied parametrically in Fig. 14. Seven cases are considered, all of which have the same parameters as Case B except for Q_{sbff} and S_{fi}, both of which have been multiplied by the same factor Q_{srat}. The values of Q_{srat} studied are 0.8, 1 (Case B), 1.4, 1.8, 2.4, 2.65 and 2.92 (Case C), corresponding to Q_{sbff} = 0.64, 0.80, 1.12, 1.44, 1.76, 2.12 and 2.336 m^3/s. Included in the plot are a) the position of the delta topset-foreset break (= shoreline) for Q_{srat} = 2.92 (Case C), and the positions of the shorelines for the other cases, plotted as functions of time.

In all cases except Q_{srat} = 2.92 the delta first progrades outward, and then slowly backsteps in autoretreat without sediment starvation. Eventually autobreak is reached, and the river mouth abandons the delta and goes into rapid sediment-starved autoretreat. Upon the cessation of sea level rise a new delta forms and progrades outward. It is seen from the figure that the extent of autoretreat is strongly dependent on the sediment supply, as quantified in terms of Q_{sbff}.

In all cases for which autoretreat is observed, the new delta progrades toward the position of the abandoned delta after the cessation of sea level rise. In only on case (Q_{srat} = 2.65) does the new delta reach and merge with the abandoned delta before t = 0 (present).

It should be noted that in the above calculation only the sand supply rate Q_{sbff} was varied (and by implication mud supply Q_{mbff}, since Λ is held constant); bankfull discharge Q_{bw} is unmodified. The relevant parameter governing the extent of autoretreat is not Q_{sbff} itself, but rather the ratio Q_{sbff}/Q_{bw}, or more familiarly the concentration of sediment in the river during floods. The mass concentration of sediment in mg/l at bankfull flow C_{mbf} is given as

$$C_{mbf} = 1x10^{-6}\,\frac{\frac{\rho_s}{\rho}(Q_{sbff}+Q_{mbff})}{Q_{bf}+Q_{sbff}+Q_{mbff}} \qquad (63)$$

where Q_{bf}, Q_{sbff} and Q_{mbff} are given in m^3/s. Assuming as before that 15% of the sediment feed is sand, C_{mbf} varies from 2480 mg/l to 7220 mg/l in the calculation of Fig. 27, the higher value preventing sediment-starved autoretreat during Pleistocene-Holocene sea level rise.

Effect of sediment load on river morphology In both cases B and C the channel sinuosity Ω has been held constant at 2.0, implying a strongly meandering river. The only differences in input between Cases B and C are in the values of sand feed rate Q_{sbff} and initial fluvial slope S_{fi}. In a natural river, however, sinuosity itself is linked to other parameters used as input in the calculation. Fisk (1944), for example, has argued that the Mississippi River, which is a strongly meandering river today, was a braided river during the earlier part of the sea level rise documented in Fig. 1. A braided stream can be expected to have a much lower sinuosity Ω than a meandering stream. Whether or not a stream meanders or braids is in turn strongly governed by the channel bankfull width-depth ratio B_{bf}/H_{bf} and downvalley bed slope S_v, here given as

$$S_v = \Omega S \tag{64}$$

(e.g. Engelund and Skovgaard, 1973; Parker, 1976; Fredsoe, 1978; Blondeaux and Seminara, 1985).

This issue is briefly studied here in terms of a hypothetical equilibrium (graded) channel associated with Cases B and C. In the case of the Fly-Strickland River system, such an approximately graded channel may have prevailed at or near the last glacial maximum, as discussed in the context of Figs. 24a-d. Calculations are performed using the relations (12) – (14) for channel bankfull characteristics and the following input parameters from Table 1: Q_{bf} = 5700 m^3/s, Cz = 25, $\tau^*_{form} = 1.82$, D = 0.25 mm and R = 1.65. Table 2 documents the computed graded values of bankfull flow velocity U_{bf}, bankfull width B_{bf}, bankfull depth H_{bf}, bankfull Froude number $\mathbf{Fr}_{bf}$, bankfull sediment concentration C_{mbf} in mg/l (sand + mud, again based on the assumption that 15% of the feed is sand), bankfull width-depth ratio B_{bf}/H_{bf}, downchannel bed slope S and downvalley slope S_v for cases B (Q_{sbbf} = 0.80 m^3/s) and C (Q_{sbff} = 2.336 m^3/s).

The values of the computed parameters for Case B all happen to be close to the values presently prevailing on the Strickland River between the gravel-sand transition and Everill Junction. This reach of the river is in fact meandering, and has a sinuosity of 2.25, i.e. close to the bulk value of 2.0 used to model Case B. The computed bankfull width-depth ratio B_{bf}/H_{bf} is 48.8.

In Case C, however, the computed value of B_{bf}/H_{bf} is 416, i.e. a value that is 8.5 times higher than Case B. In increase in B_{bf}/H_{bf} from 48.8 to 416 can be expected to push stream morphology strongly in the direction of a braided sand-bed stream such as the present-day Brahmaputra River, Bangladesh. With this in mind, Case C was modified to Case C' for which the sinuosity was lowered to 1.2, as documented in Table 2. Also shown in Table 2 is the valley slope S_v for Case C', which at 0.000357 is 1.75 time higher than the value for Case B.

The values of (B_{bf}/H_{bf}, S_v) for Case C' are thus (8.5, 1.75) times higher than Case B. A calculation was performed for Case C' in which in addition to the modifications of Q_{sbff} and Ω, the initial downchannel reach length s_{tfi} was reduced from 970 km to 582 km in order to ensure that both Cases B and C describe a river with the same initial valley distance from the gravel-sand transition to the shelf edge. The results were qualitatively no different than those for the original Case C; again the delta did not go into sediment-starved autoretreat.

The calculations for Case B indicate that the ratio B_{bf}/H_{bf} never exceeds 50, i.e. a value close to its present value, throughout 21000 years of calculation. This provides a partial *a posteriori* justification of the assumption that the river was meandering at low stand and remained so throughout Pleistocene-Holocene sea level rise to the present day.

CONCLUSIONS AND CAVEATS

Conclusions The main conclusions of this analysis are outlined below.

1. As illustrated in the companion paper, Part I, the small-scale experiments of Muto (2001), and in particular the phenomenon of sediment-starved autoretreat identified therein, is of direct relevance to the response of large sand-bed rivers to Pleistocene-Holocene sea level rise.

2. An appropriately modified version of the moving boundary formulation of Swenson et al. (2000) provides a framework for a numerical model that can encompass both the experiments of Muto (2001) and large sand-bed rivers. The most important adaptation is a quantification of the morphodynamics of bedrock-alluvial transitions.

3. Such a numerical model can capture with reasonable accuracy the river response to sea level rise modeled experimentally by Muto (2001). In

particular, it can capture the phenomenon of drowning of the river mouth during sediment-starved autoretreat.

4. The introduction of a number of modifications allow adaptation of the numerical model to field sand-bed rivers. The more innovative of these include:

- Use of a channel-forming Shields number to quantitatively describe self-formed channels for which bed slope, bankfull width and bankfull depth are all dependent variables;
- Adaptation of the treatment to include backwater effects, and adaptation of the backwater formulation to describe channels that maintain a set channel-forming Shields number;
- Introduction of a criterion for the drowning of the channel during sediment-starved autoretreat; and
- Modification of the equation of sediment conservation to describe washload (mud) as well as bed material load (sand), and to describe the co-evolution of the channel/floodplain complex under net depositional conditions;

5. The adapted numerical model allows for quantitative predictions of the effect of sea level rise on large sand-bed rivers as long as appropriate input parameters can be reasonably estimated. An example of such a calculation is presented for the Fly-Strickland River System.

6. The model applied at field scale suggests that the effect of Pleistocene-Holocene sea level rise on the Fly-Strickland River system was likely profound, and likely propagated as far upstream as the present-day gravel-sand transition.

The predicted values of river aggradation in the reach between Everill Junction and the gravel-sand transition are more than sufficient to create the present-day blocked-valley Lake Murray.

7. The same application of the model suggests that Pleistocene-Holocene sea level rise forced the mouth of the Fly-Strickland River into over 700 km of sediment-starved autoretreat, and that the Fly Estuary may be to a large degree a consequence of the resulting drowning of the river valley.

8. Sediment-starved autoretreat forces considerably more rapid shoreline transgression and more substantial riverbed aggradation that propagates much farther upstream of that produced by autoretreat without sediment starvation.

9. The approximate correspondence between the predicted position of the present-day delta of the Fly River and the observed point at which the river gives way to an estuary suggests that the river may presently be constructing a new self-formed channel into the estuary as it recovers from Pleistocene-Holocene sea level rise.

10. If the same river system subjected to the same sea level rise curve has a higher sediment feed rate, the degree to which the stream undergoes autoretreat is reduced. For a sufficiently high sediment feed rate the river delta could have continued to prograde throughout Pleistocene-Holocene sea level rise.

11. Sediment feed concentration thus strongly influences the degree to which a river mouth transgresses for a given curve of sea level rise. With all other factors equal, a river with a sufficiently high feed concentration would be

expected to end in a prograding delta protruding into the sea today, whereas a river with a sufficiently low feed concentration would be expected to end in a delta contained in an estuary that intrudes landward from the general shoreline.

Caveats The analysis reported here has been performed at relatively a high level of quantification and detail compared to previous models of the effect of sea level rise on rivers in particular and margins in general (e.g. Jordan and Flemings, 1991). Having said this, the analysis still remains broad-brush compared to real rivers. It is thus of use to enumerate briefly a number of caveats concerning the model.

- The model assumes constant values of bankfull discharge, flood intermittency, feed rates of sand and mud and sand grain size over a time span of 21000 years, from the last glacial maximum until today. While this is unlikely to be true, it is likely less of an error for the case of New Guinea than a region at a higher latitude that was subjected to floods resulting from the melting of continental glaciers. The input parameters can be modified as more information about climate change becomes available.
- The model assumes a river slope at low stand at the beginning of the calculation that is equal to the observed present slope, i.e. 0.0001. While there appears to be little doubt that the Strickland River aggraded in response to sea level rise, the predicted aggradation of ~ 50 m near Lake Murray appears high. This suggests that the river slope at low stand may have been higher than the present-day value.

- The model does not include downstream fining. This aspect can be remedied with the formulation of Wright and Parker (in press(a),(b) (c)).
- The model assumes constant floodplain width, includes no tributaries, and does not account for increasing discharge in the downstream direction due to rainfall on the floodplain. All of these factors could be addressed with appropriate changes in data input.
- A gravel-sand transition is not synonymous with a bedrock-alluvial transition. Gravel deposition at the transition acts to resist upstream migration. As a result the model likely overpredicts upstream migration of the gravel-sand transition. This issue can be addressed by introducing a gravel-sand transition, at the expense of adding complexity to the model.
- The present-day gravel-sand transition of the Strickland River also appears to be located at a hinge between uplift and subsidence. Uplift/subsidence is not included in the present model. It could be included using, for example, the formulation of Swenson et al. (2000). Uplift of the reach upstream of the gravel-sand transition would also reduce the upstream migration of this point.
- No tidal effects are included in the model, nor is mud allowed to deposit in the estuary. The effect of tides would be to smear out the sand delta and draw sand well into the present-day Fly Estuary. By increasing the delivery of sand to the Fly Estuary, tides could also reduce, perhaps substantially, the amount of aggradation experienced by the river upstream. The inclusion of tides in the model is technically possible, but

would require an extremely short time step (much smaller than a single tidal cycle) over a calculation period of 21000 years. The deposition of mud in the estuary would also substantially reduce the height of any delta. The work of Kostic and Parker (2003a,b) and Swenson *et al.* (2005) suggest ways to address the issue of mud deposition beyond the delta.

- Tidal effects have also likely strongly influenced the present-day funnel-shaped morphology of the Fly Estuary, an issue that is not addressed by the model.
- The Pleistocene-Holocene sea level rise did not occur at a constant rate of 10 mm/year over 12000 years, as approximated here. The curve of Fig. 1 due to Bard et al. (1996) includes one step associated with meltwater pulse 1A at about 14000 years BP, and the work of Webster et al. (2004) suggests multiple steps. Work is in progress to generalize the analysis to stepped sea level curves.
- The present analysis is quasi-one-dimensional. It cannot represent changes in deltaic depocenter over scales larger than one floodplain width, and also cannot represent the two-dimensional phenomenon of autostepping during transgression observed by Muto and Steel (2001). The work of Sun et al. (2002) offers a possibility for generalizing the model in this direction.
- Some evidence suggests that the Strickland River not only created Lake Murray by valley blocking, but may have actually blocked part of the lower

Middle Fly River during at least part of the Pleistocene-Holocene sea level rise. This issue is being investigated separately.

In summary, the model presented here should be interpreted as representing the first step in a quantitative determination of the effect of sea level rise on a large river. Many improvements and modifications can be expected in the future.

The numerical calculations reported here were performed using code written in Visual Basic for Applications, and embedded in an Excel workbook. One of the spreadsheets of the workbook constitutes the Graphical User Interface. The workbook is available from the first author upon request.

ACKNOWLEDGEMENTS

This paper and the companion paper, Parker et al. (submitted) include material from two papers in conference proceedings: Parker and Muto (2003) and Parker et al. (2004). The scope of the research has been greatly extended in the present paper. A personal communication from T. Törnqvist in December of 2003 proved valuable. Bathymetric information for the Gulf of Papua was provided by C. Nittrouer.

This research was funded by the National Science Foundation Source to Sink Program (Collaborative Research: Processes Controlling Depositional Signals of Environmental Change in the Fly River Sediment Dispersal System: Rates and Mechanisms of Floodplain Deposition, EAR-0203296) and the National Center for Earth-surface Dynamics (NCED), a National Science Foundation Science and Technology Center (EAR-0120914). This paper is a contribution of the research effort of NCED in the area of channel dynamics. The participation of Y. Akamatsu was enabled by a grant from the Japan Society for the Promotion of Science.

REFERENCES

Bard, E., Hamelin, B., Arnold, M., Montaggioni, L., Cabioch, G., Faure, G. and **Rougerie, F.** (1996) Deglacial sea-level record from Tahiti corals and the timing of global meltwater discharge. *Nature*, 382, pp. 241-244.

Blondeaux, P. and Seminara, G. (1985) A unified bar-bend theory of river meanders. *Journal of Fluid Mechanics*, **157**, 449-470.

Blum, M. B. and **Törnqvist, T. E.** (2000) Fluvial responses to climate and sea-level change: a review and look forward. *Sedimentology*, **47** (Suppl. 1), 2-48.

Brownlie, W. R. (1981) Prediction of flow depth and sediment discharge in open channels. *Report* No. KH-R-43A, W. M. Keck Laboratory of Hydraulics and Water Resources, California Institute of Technology, Pasadena, California, USA, 232 p.

Cui, Y. and **Parker**, G. (1999). Sediment transport and deposition in the Ok Tedi-Fly River System, Papua New Guinea; the modeling of 1998-1999. *Report*, Ok Tedi Mining Ltd.

Dietrich, W. E., Day, G. and **Parker, G.** (1999) The Fly River, Papua New Guinea: inferences about river dynamics, floodplain sedimentation and fate of sediment. In *Varieties of Fluvial Form*, Miller, A. J. and Gupta, A., eds., John Wiley and Sons, New York, 345-376.

Engelund, F. and **Hansen, E.** (1967) *A Monograph on Sediment Transport in Alluvial Streams*, Technisk Vorlag, Copenhagen, Denmark.

Engelund, F. and Skovgaard, O. (1973) On the origin of meandering and braiding in alluvial streams. *Journal of Fluid Mechanics*, **57**, 289-302.

Fisk, H. N. (1944) *Geological Investigation of the Alluvial Valley of the Lower Mississippi River*, Mississippi River Commission, Vicksburg.

Fredsoe J. (1978) Meandering and braiding of rivers. *Journal Fluid Mechanics*, **84**, 609-624.

Henderson, F. M. (1966) *Open Channel Flow*. Macmillan, New York.

Higgins, R. (1990) Off-river storages as sources and sinks for environmental contaminants. *Regulated Rivers*, **5**, 401-412.

Hope, G.S. and **Peterson, J.A.** (1975) Glaciation and vegetation in the high New Guinea Mountains. *Bull. Roy. Soc. N.Z.*, **13**, 155-162.

Jordan, T. E. and **P. B. Flemings** (1991) Large-scale stratigraphic architecture, eustatic variation, and unsteady tectonism: A theoretical evaluation. *Journal of Geophysical Research* **96**, 6681-6699.

Kostic, S. and Parker, G. (2003a) Progradational sand-mud deltas in lakes and reservoirs. Part I. Theory and numerical modeling. *Journal of Hydraulic Research*, **41(2)**, 127-140.

Kostic, S. and Parker, G. (2003b) Progradational sand-mud deltas in lakes and reservoirs. Part 2. Experiment and numerical simulation. *Journal of Hydraulic Research*, **41(2)**, 141-152.

Loffler, H. (1973) Tropical high mountain lakes of New Guinea and their zoogeographical relationship compared with other tropical high mountain lakes. *Arctic and Alpine Research*, **5(3)**, Part 2, A193-A198.

Muto, T. (2001) Shoreline autoretreat substantiated in flume experiment. *Journal of Sedimentary Research*, **71(2)**, 246-254.

Muto, T. and **Steel, R. J.** (2001) Autostepping during the transgressive growth of deltas: Results from a flume experiment. *Geology*, **29(9)**, 771-774.

Paola, C., **Heller, P.L.** and **Angevine, C.L.**, (1992) The large-scale dynamics of grain-size variation in alluvial basins, 1: Theory. **Basin Research 4**, 73-90.

Parker, G. (1976) On the cause and characteristic scales of meandering and braiding in rivers. *Journal of Fluid Mechanics*, **76**, 457-480.

Parker, G., Paola, C., Whipple, K. X. and **Mohrig, D.** (1998) Alluvial fans formed by channelized fluvial and sheet flow. I: Theory. *Journal of Hydraulic Engineering*, **124(10)**, 985-995.

Parker, G. and **Toro-Escobar, C. M.** (2002) Equal mobility of gravel in streams: The remains of the day. *Water Resources Research*, **38(11)**, 1264, doi: 10.1029/2001WR000669.

Parker, G. and **Muto, T.** (2003) 1D numerical model of delta response to rising sea level, *Proceedings*, 3rd IAHR Symposium, River, Coastal and Estuarine Morphodynamics, Barcelona, Spain, September 1-5., 10 p.

Parker, G., Akamatsu, Y., Muto, T. and **Dietrich, W.** (2004) Modeling the effect of rising sea level on river deltas and long profiles of rivers. *Proceedings*, International Conference on Civil and Environmental Engineering ICCEE-2004, Hiroshima University, Higashi-Hiroshima, Japan, July 27-28, 1-11.

Parker, G., Muto, T., Akamatsu, Y., Dietrich, W. E. (submitted) Unraveling the conundrum of river response to rising sea level from laboratory to field. Part I. Laboratory experiments. *Sedimentology.*

Peterson, J., Hope, G., Prentice, M. and **Hantoro, W.** (2002) Mountain environments in New Guinea and the late Glacial Maximum 'warm seas/cold mountains' enigma in the West Pacific Warm Pool region. *Advances in Geoecology,* **34**, 173-188.

Pickup, G. (1984) Geomorphology of tropical rivers, I. Landforms, hydrology and sedimentation in the Fly and lower Purari, Papua New Guinea, *Catena* Suppl. 5, pp. 1-17.

Richards, K. (1982) *Rivers: form and process in alluvial channels*. Methuen, London and New York, ISBN 0-416-74900-3, 358 p.

Sun, T., Paola, C., Parker, G. And **Meakin, P.** (2002) Fluvial fan-deltas: Linking channel processes with large-scale morphodynamics. *Water Resources Research*, **38**(2), doi:10.1029/2001WR000284.

Swenson, J. B., Voller, V. R., Paola, C., Parker, G. and **Marr, J.** (2000) Fluvio-deltaic sedimentation: A generalized Stefan problem. *European Journal of Applied Math*., **11**, 433-452.

Swenson, J. B., Paola, C., Pratson, L., Voller, V. R. and Murray, A. B. (2005) Fluvial and marine controls on combined subaerial and subaqueous delta progradation: Morphodynamic modeling of compound clinoform development. *Journal of Geophysical Research*, **110**, F02013, doi:10.1029/2004JF000265, 16 p.

Törnqvist, T. (1993) Fluvial sedimentary geology and chronology of the holocene Rhine-Meuse Delta, the Netherlands. Ph.D. thesis, Utrecht University, the Netherlands.

Törnqvist, T. (2003) Personal communication concerning the fraction of sand, mud and organics in the floodplain deposits of the Rhine River, the Netherlands.

Webster, J. M. Clague, D. A. Riker-Coleman, K., Gallup, C., Braga, J. C., Potts, D., Moore, J. G., Winterer, E. L. and **Paull, C. L.** (2004) Drowning of the – 150 m reef off Hawaii: A casualty of global meltwater pulse 1A? *Geology*, **32**(3), 249-252.

Wright, S. and Parker, G. (2004a) Density stratification effects in sand-bed rivers. *Journal of Hydraulic Engineering*, 130(8), 783-795..

Wright, S. and Parker, G. (2004b) Flow resistance and suspended load in sand-bed rivers: simplified stratification model. *Journal of Hydraulic Engineering*, 130(8), 796-805.

Wright, S. and Parker, G. (2005a) Modeling downstream fining in sand-bed rivers. I: Formulation. *Journal of Hydraulic Research*, 43(6), 612-619.

Wright, S. and Parker, G. (2005b) Modeling downstream fining in sand-bed rivers. II: Application. *Journal of Hydraulic Research*, 43(6), 620-630.

NOMENCLATURE

Symbol	Meaning	Dimensions (**L** length, **M** mass, **T** time, (1 dimensionless)
B_{bf}	Bankfull channel width	**L**
$\hat{B}$	Dimensionless bankfull width given by (8c)	1
B_f	Width of floodplain (valley)	**L**
C_f	Dimensionless bed friction coefficient defined by (2c)	1
C_{mbf}	Bankfull sediment concentration in mg/l	$\mathbf{ML^{-3}}$
Cz	$= 1/\sqrt{C_f}$, dimensionless Chezy friction coefficient	1
Cz_{bf}	Value of Cz at bankfull flow	1
D	Characteristic (median or geometric mean) sediment grain size	**L**
$\mathbf{Fr}_{bf}$	Dimensionless Froude number at bankfull flow, defined by (20)	1
g	Gravitational acceleration	$\mathbf{LT^{-2}}$
H	River depth	**L**
H_{bf}	Bankfull value of H	**L**
$\hat{H}$	Dimensionless bankfull depth given by (8b)	1

I_f	Flood intermittency	**L**
i	Index denoting either the ith spatial node or the initial value of a parameter	1
M_{sand}	Mean annual mass transport rate of sand	$\mathbf{MT^{-1}}$
M_{sandf}	Mean annual mass feed rate of sand	$\mathbf{MT^{-1}}$
M_{sed}	Mean annual mass transport rate of sediment (sand + mud)	$\mathbf{MT^{-1}}$
M_{sedf}	Mean annual mass feed rate of sediment (sand + mud)	$\mathbf{MT^{-1}}$
N	Number of intervals in spatial discretization	1
Q_{bf}	Bankfull water discharge	$\mathbf{L^3T^{-1}}$
$\hat{Q}$	Dimensionless bankfull discharge given by (8a)	1
Q_{mbf}	Volume mud transport rate excluding pores at bankfull flow	$\mathbf{L^3T^{-1}}$
Q_{mbff}	Volume feed rate of mud excluding pores at bankfull flow excluding pores	$\mathbf{L^3T^{-1}}$
Q_{sbf}	Volume sand transport rate excluding pores at bankfull flow	$\mathbf{L^3T^{-1}}$
$\hat{Q}_s$	Dimensionless bankfull sand discharge given by (10a)	1
Q_{sbff}	Volume sand feed rate excluding pores at bankfull flow	$\mathbf{L^3T^{-1}}$
Q_{srat}	Ratio of Q_{sbff} to the value 0.80 m^3/s used in Cases A and B of the calculations	1
q^*	Dimensionless Einstein number defined by (2a)	1
q_s	Volume sand transport rate per unit width excluding pores	$\mathbf{L^2T^{-1}}$
q_{sbf}	Value of q_s at bankfull flow	$\mathbf{L^2T^{-1}}$
q_w	Water discharge per unit width	$\mathbf{L^2T^{-1}}$
q_{wbf}	Bankfull value of q_w	$\mathbf{L^2T^{-1}}$
R	= $(\rho_s/\rho - 1)$, submerged specific gravity of sediment (~ 1.65 for quartz)	1
r_S	critical value of the ratio S_{fric}/S below which the valley is assumed to be drowned	1
S	= $-\partial\eta/\partial x$, local alluvial bed slope	1
S_{aba}	Alluvial slope at bedrock-alluvial transition	1
S_{bb}	Subaerial basement slope to which alluvial river reach onlaps	1
S_{sb}	Subaqueous basement slope over which river delta progrades	1
S_{fric}	Bankfull friction slope given by (19) or (23b)	1
S_{fi}	Initial slope of fluvial region	1
S_{fore}	Foreset slope (assumed constant here)	1

S_{ttf}	Alluvial topset slope at topset-foreset break	1
S_u	Alluvial bed slope at bedrock-alluvial transition	1
S_v	= ΩS, valley slope	1
s_{ba}	Position of bedrock-alluvial transition	**L**
$\dot{s}_{ba}$	Migration speed of bedrock-alluvial transition	$\mathbf{LT^{-1}}$
s_{sb}	Position of foreset-subaqueous basement break	**L**
s_{sbi}	Initial value of s_{sb}	**L**
$\dot{s}_{sb}$	Migration speed of foreset-subaqueous break	$\mathbf{LT^{-1}}$
s_{tf}	Position of topset-foreset break	**L**
s_{tfi}	Initial value of s_{tf}	
$\dot{s}_{tf}$	Migration speed of topset-foreset break	$\mathbf{LT^{-1}}$
t	Time	**T**
$\bar{t}$	Moving boundary time coordinate given by (21b)	**T**
U	= q_w/H, depth-averaged river flow velocity	$\mathbf{LT^{-1}}$
U_{bf}	Bankfull value of U	$\mathbf{LT^{-1}}$
x	Downchannel streamwise coordinate	**L**
x_v	Downvalley streamwise coordinate	**L**
$\bar{x}$	Dimensionless moving boundary spatial coordinate given by (21a)	1
$\Delta\bar{x}$	Interval length in discretization of $\bar{x}$	1
$\Delta\bar{t}$	Step length in time $\bar{t}$	**T**
$\Delta\eta$	Elevation drop across the foreset	**L**
$\Delta\eta_i$	Initial value of $\Delta\eta$	**L**
η	Local alluvial bed elevation	**L**
η_{bi}	Initial elevation of the foreset-subaqueous basement break	**L**
η_{base}	Local basement elevation	**L**
η_s	Bed elevation at the shoreline	**L**
η_{ti}	Initial elevation of the topset-foreset break	**L**
Λ	Volume unit of mud deposited in the channel-floodplain complex per unit sand deposited	1
λ_p	Porosity of deposit	1
ρ	Density of water	$\mathbf{ML^{-3}}$
ρ_s	Density of sediment	$\mathbf{ML^{-3}}$
τ^*	Dimensionless Shields number defined by (2b)	1
τ^*_{bf}	Shields number at bankfull flow given by (10b)	1
τ^*_{form}	Channel-forming Shields number	1
τ_b	Bed shear stress	$\mathbf{ML^{-1}T^{-2}}$

τ_{bbf}	Bankfull value of τ_b	$\mathbf{ML^{-1}T^{-2}}$
Ω	Channel sinuosity	1
ξ	Sea level or elevation of standing water (base level)	**L**
ξ_i	Initial value of ξ	**L**
$\dot{\xi}$	Rate of rise of sea level or elevation of standing water	$\mathbf{LT^{-1}}$

TABLE 1 PARAMETERS USED TO MODEL THE FLY-STRICKLAND RIVER SYSTEM

Parameter	Value	Units	Description	Notes
Q_{bf}	5700	m^3/s	Bankfull discharge	Estimated from gaging stations on Strickland and Fly Rivers (Obo and SG4).
I_f	0.175		Flood intermittency	Estimate based on the Fly River near D'Albertis Junction, a reach with similar characteristics.
Q_{sbff}	0.80	m^3/s	Sand feed rate during floods	Back-calculated from data and equations for channel geometry: used for Cases A and B. For Case C the value is increased by a factor of 2.92 to 2.336 m^3/s.
M_{sandf}	11.7	Mt/a	Mean annual sand feed rate	Value for Cases A and B based on comments immediately above.
M_{sedf}	78.1	Mt/a	Mean annual sediment (sand + mud) feed rate	Based on above value of M_{sandf} and the assumption that 15% of the sediment feed is sand.
Λ	1.0		Mud/sand deposition ratio	Reasonable guess motivated by personal communication from T. Törnqvist.
Ω	2.0		Channel sinuosity	Average based on estimates from satellite photographs.
Cz_{bf}	25		Chezy bed resistance coefficient	Back-calculated from data and equations for channel geometry.
D	0.25	mm	Characteristic sand grain size	Sediment survey of Strickland River at Ogwa.
B_f	12000	m	Floodplain width	Average based on estimates from aerial and satellite photographs.
s_{fi}	970000	m	Initial downchannel length of alluvial topset reach	Chosen to yield a final distance from the bedrock-sand transition to the shelf edge of 113000 m based on aerial and satellite photographs.
S_{fi}	0.0001		Initial downchannel slope of fluvial topset reach	Reasonable inference based on available data on Strickland river below gravel-sand transition. This value is used for Cases A and B; in case C the value is increased to 0.000292.
S_{bb}	0.00046		Slope of subaerial bedrock reach	From SRTM data for gravel-bed reach near gravel-sand transition.
S_{sb}	0.00075		Slope of subaqueous basement	From available bathymetric data.
S_{fore}	0.0016		Slope of foreset	From available bathymetric data.
ξ_i	-120	m	Initial sea level	From available bathymetric data; datum is present-day sea level.
η_{ti}	-130	m	Initial elevation of topset-foreset break	Value chosen to yield an initial depth of 10 m at topset-foreset break.
η_{bi}	-170	m	Initial elevation of foreset-subaqueous basement break	From available bathymetric data.
λ_p	0.35		Porosity of channel/floodplain complex	Reasonable estimate for a deposit consisting of half sand and half mud that has compacted over thousands of years.
R	1.65		Submerged specific gravity of sediment	Value for quartz.
τ^*_{form}	1.82		Channel-forming Shields number	Back-calculated from data and equations for channel geometry.

TABLE 2 CALCULATED PARAMETERS FOR GRADED CHANNEL

Parameter	Description	Case B	Case C	Case C’
U_{bf} (m/s)	Bankfull flow velocity	2.15	2.15	2.15
B_{bf} (m)	Bankfull width	360	1052	1052
H_{bf} (m)	Bankfull depth	7.38	2.52	2.52
$\mathbf{Fr}_{bf}$	Bankfull Froude number	0.252	0.431	0.431
C_{mbf} (mg/l)	Sediment concentration	2477	7221	7221
B_{bf}/H_{bf}	Bankfull width-depth ratio	48.8	416	416
S	Downchannel bed slope	0.000102	0.000297	0.000297
Ω	Channel sinuosity	2.0	2.0	1.2
S_v	Valley slope	0.000204	0.000594	0.000357

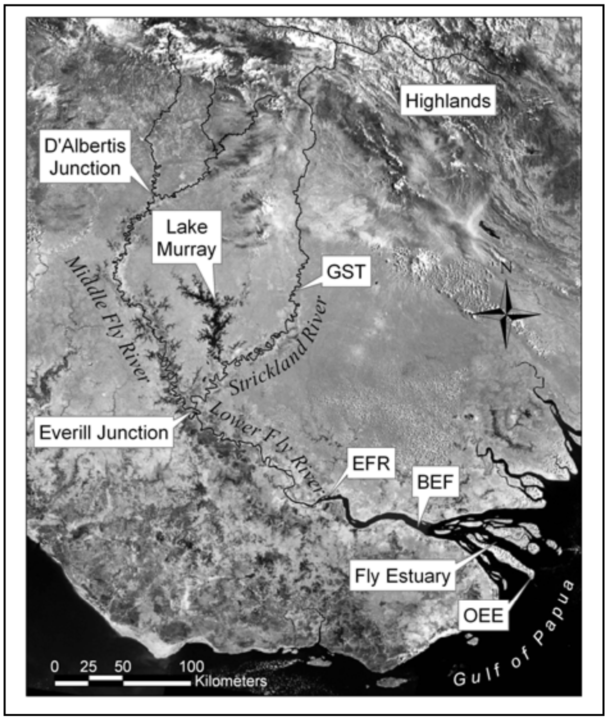

Figure 1. Annotated satellite image of the Fly-Strickland River System, Papua New Guinea. The abbreviations GST, EFR, BEF and OEE denote “gravel-sand transition,” “end of fluvial reach,” “beginning of estuary flare,” and “outer edge of estuary,” respectively. The image is from the NASA web site, https://zulu.ssc.nasa.gov/mrsid/.

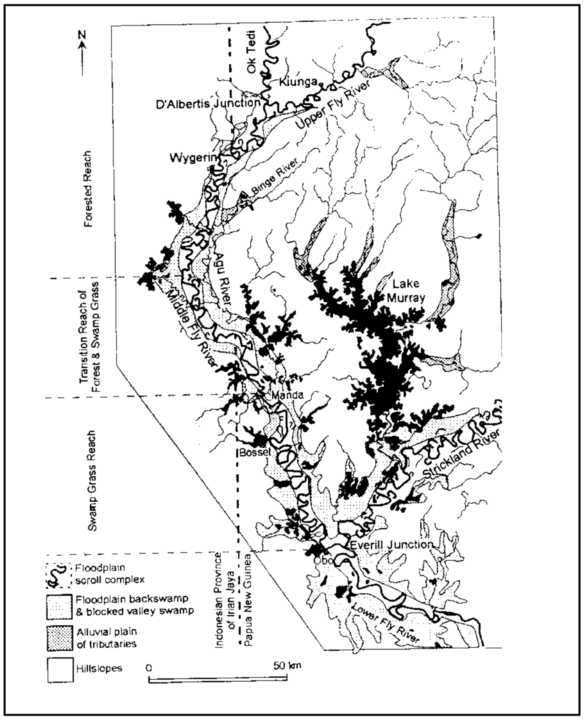

Figure 2. Sketch of part of the Fly-Strickland River System showing numerous blocked-valley lakes. From Dietrich et al. (1999).

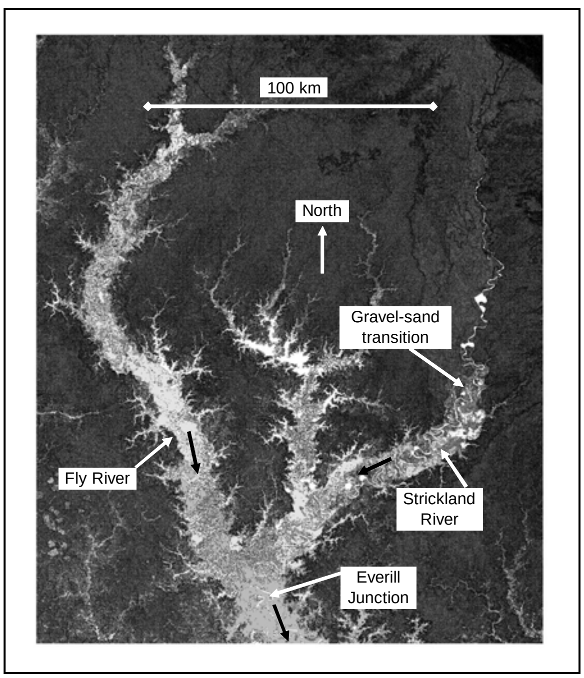

Figure 3. SRTM (Shuttle Radar Topographic Mission) image of the Fly-Strickland River system. The lighter shading denotes the river floodplain. The approximate position of the gravel-sand transition on the Strickland River is shown.

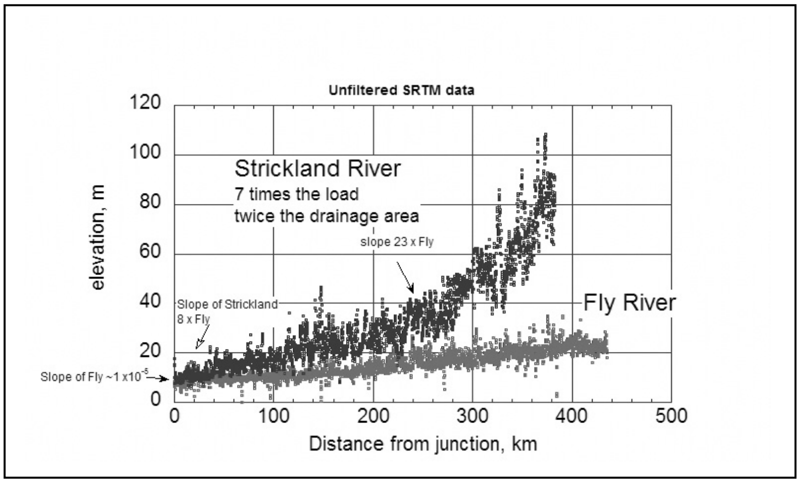

Figure 4. Long profiles of the Strickland and Fly River bank elevations upstream of Everill Junction. Elevations were obtained from SRTM (Shuttle Radar Topographic Mission) data.

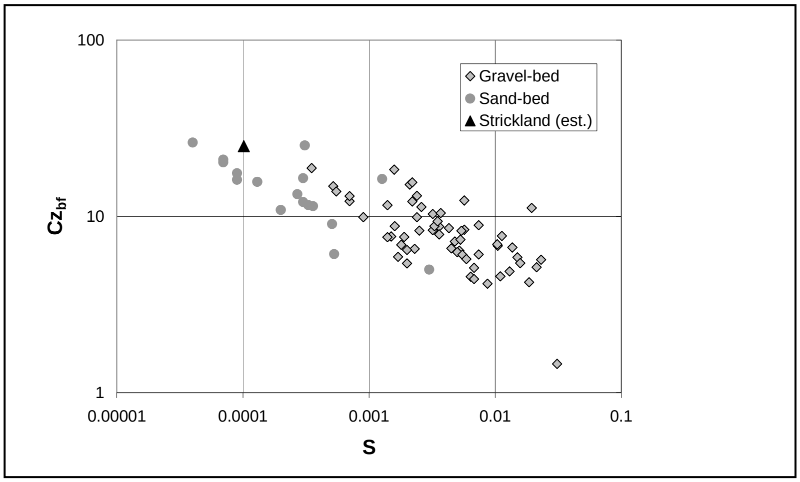

Figure 5. Plot of bankfull Chezy friction coefficient Cz_{bf} as a function of bed slope S for selected sand-bed and gravel-bed streams.

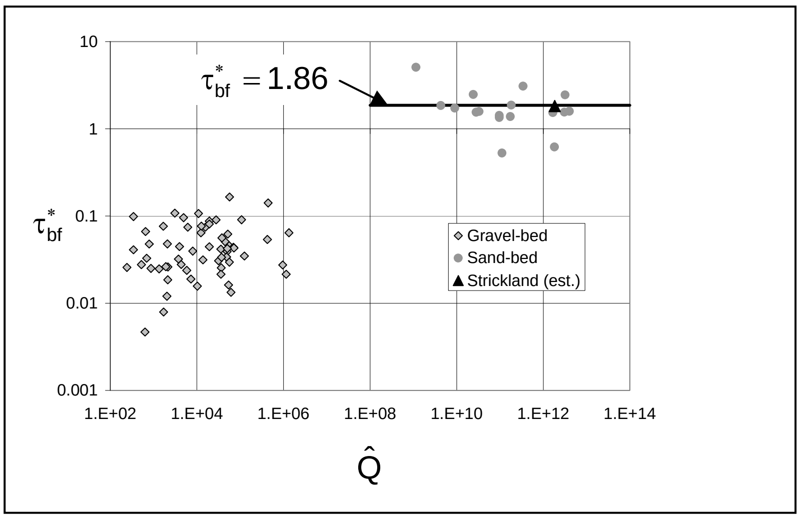

Figure 6. Plot of bankfull Shields number τ^*_{bf} as a function of dimensionless bankfull discharge $\hat{Q}$ for selected sand-bed and gravel-bed streams.

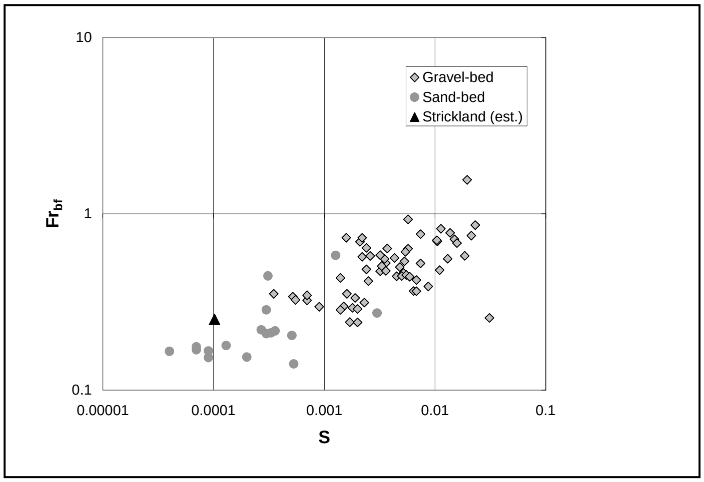

Figure 7. Plot of bankfull Froude number $\mathbf{Fr}_{bf}$ as a function of bed slope S for selected sand-bed and gravel-bed streams.

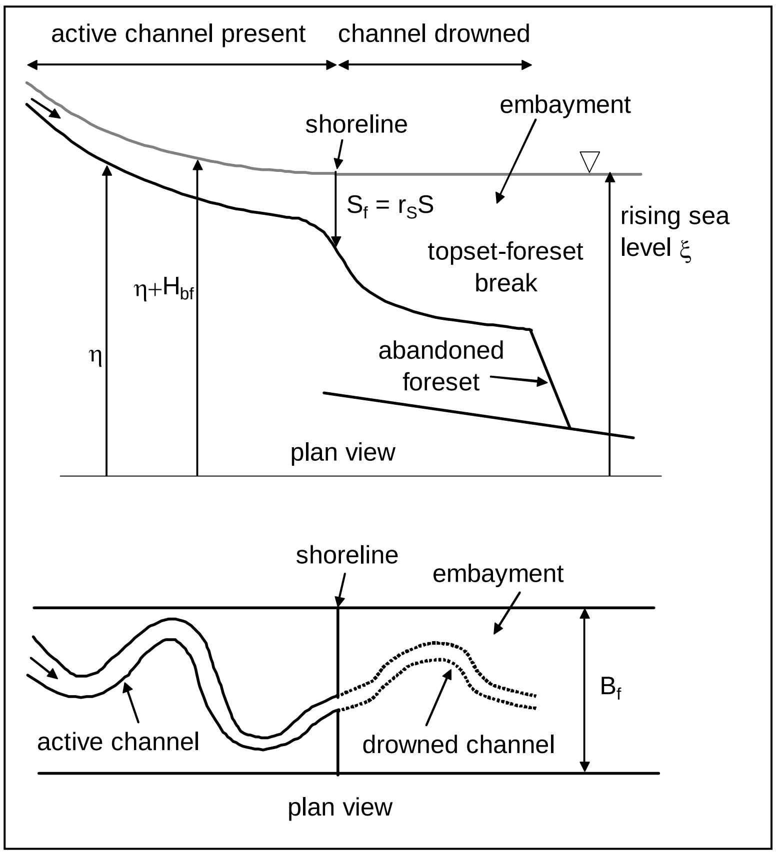

Figure 8. Diagram illustrating the decoupling of the shoreline from the topset-foreset break for the case of a self-formed channel subject to sediment-starved autoretreat.

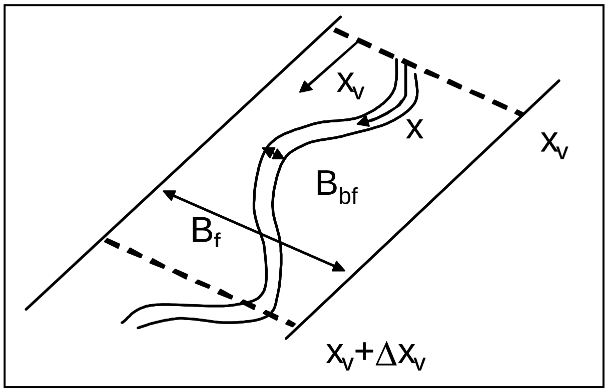

Figure 9. Definition diagram for the derivation of the Exner equation of sediment continuity for a co-evolving channel-floodplain complex.

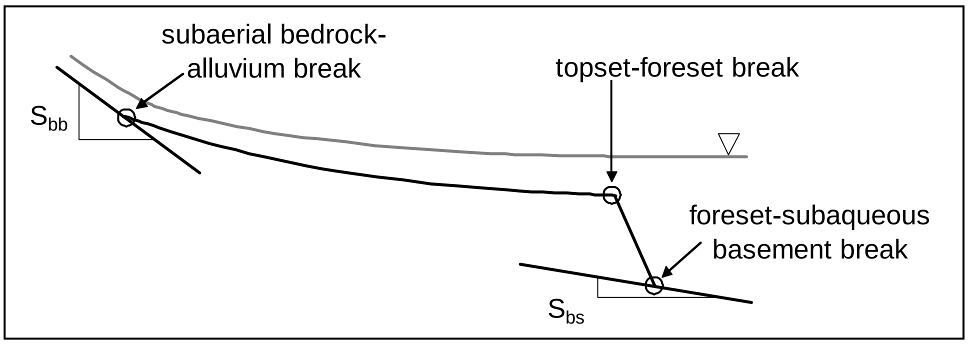

Figure 10. Illustration of the use of two basement slopes, one subaerial and one subaqueous, in describing the evolution of a river flowing into the sea.

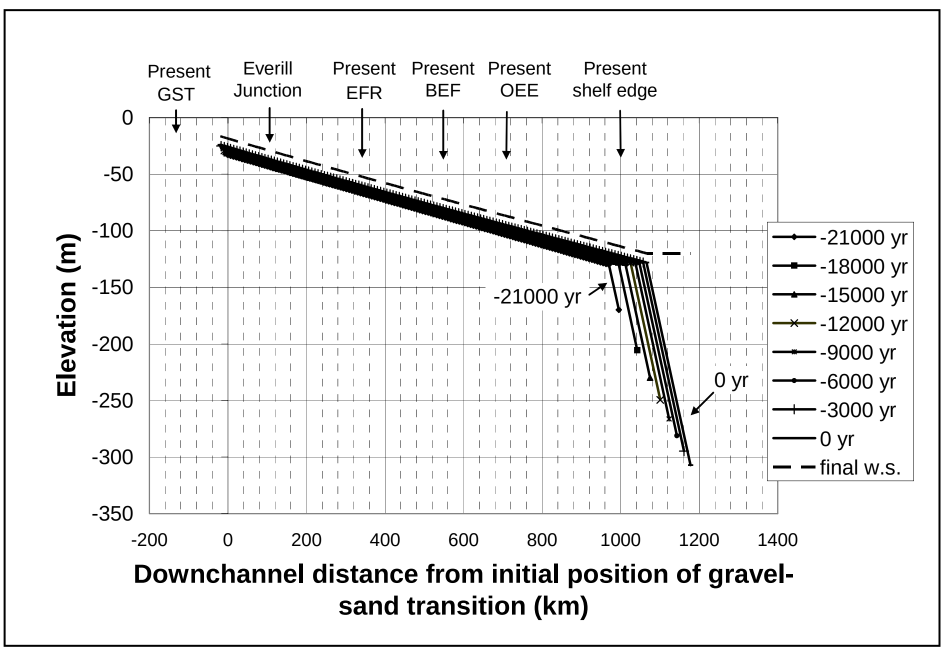

Fig. 11a. Profiles of bed elevation every 3000 years and final water surface elevation for Case A. The abbreviations "GST," "EFR," "BEF" and "OEE" are explained in the caption of Fig. 14.

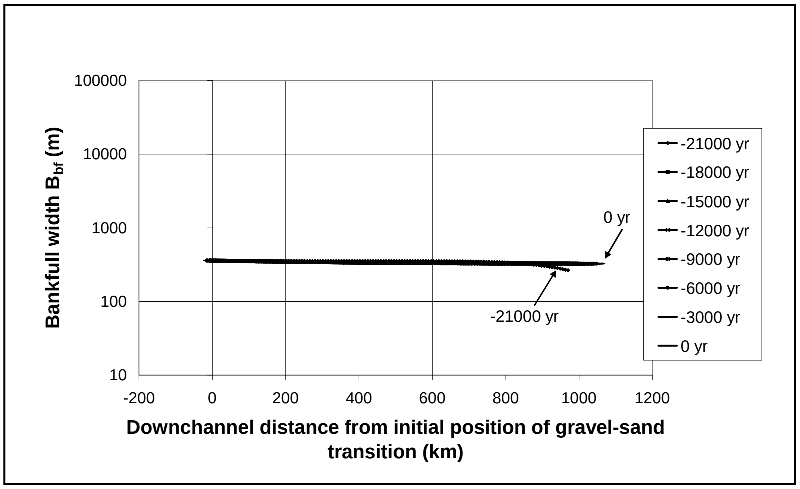

Fig. 11b. Profiles of bankfull width B_{bf} every 3000 years for Case A.

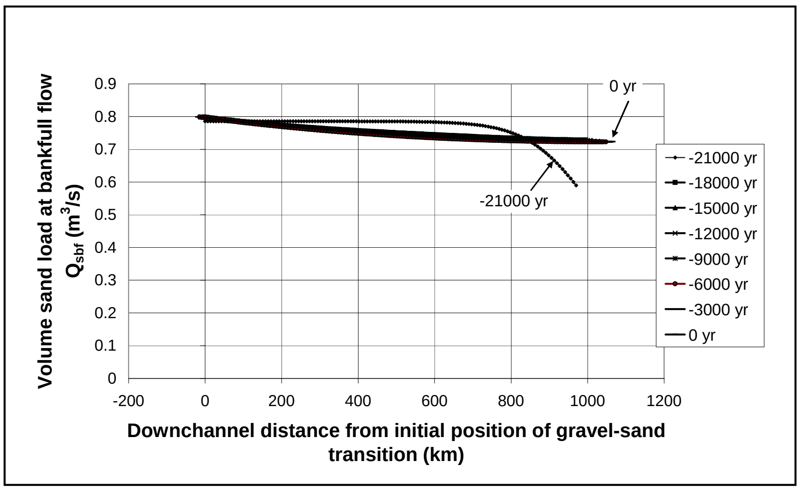

Fig. 11c. Profiles of volume sand transport rate at bankfull Q_{sbf} flow every 3000 years for Case A.

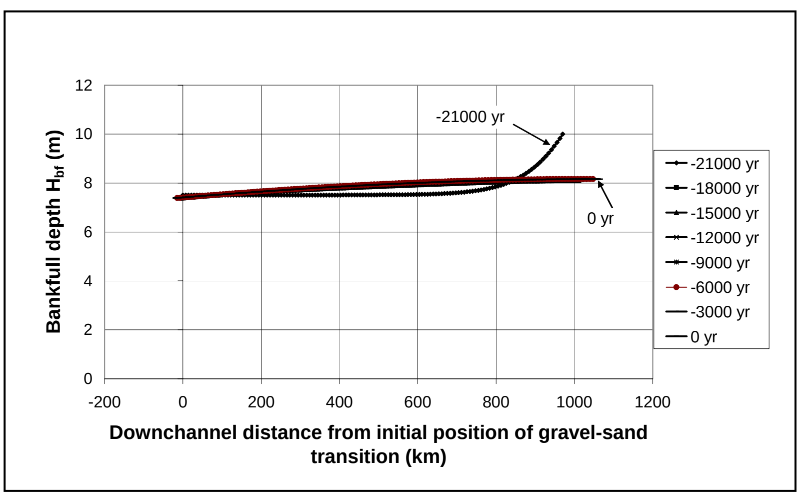

Fig. 11d. Profiles of bankfull depth H_{bf} every 3000 years for Case A.

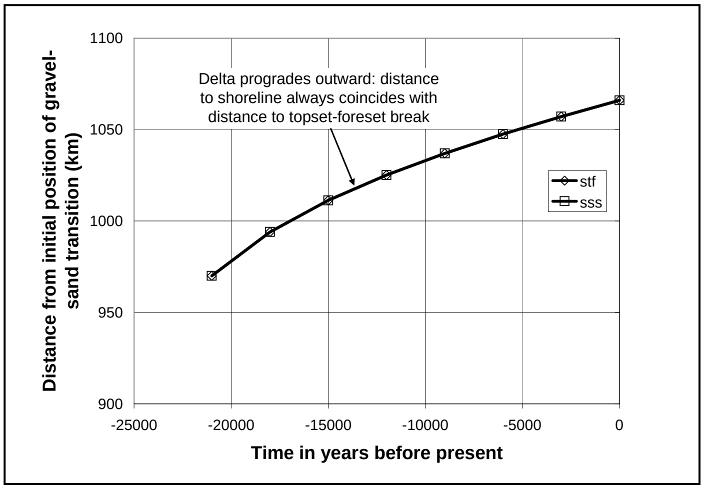

Fig. 11e. Plot of downchannel distance from the initial position of the gravel-sand transition to a) the delta topset-foreset break (stf) and b) the shoreline (sss) for Case A. The delta is never abandoned because sea level is constant in Case A.

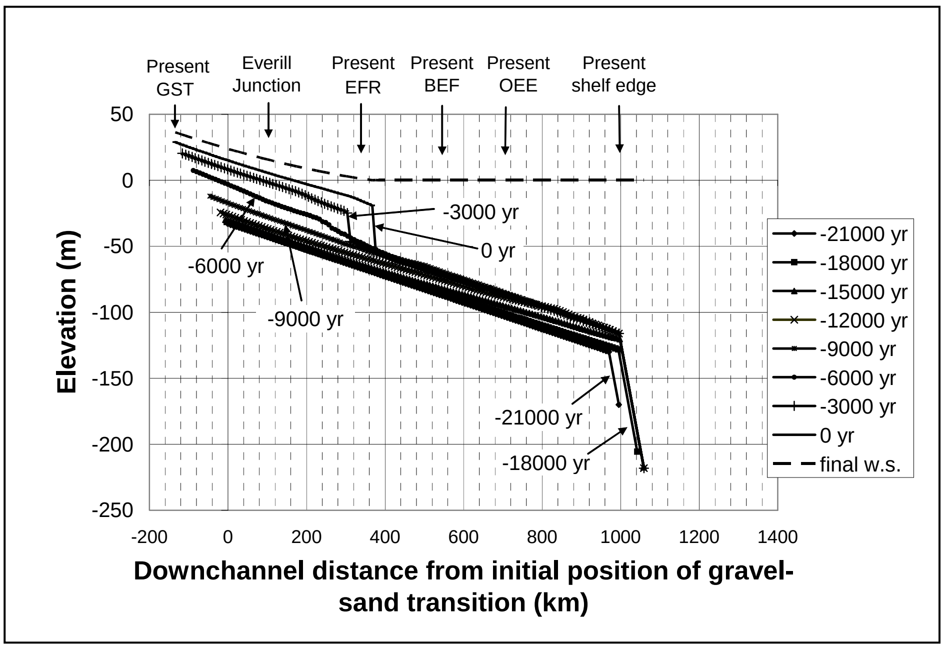

Fig. 12a. Profiles of bed elevation every 3000 years and final water surface elevation for Case B. The abbreviations “GST,” “EFR,” “BEF” and “OEE” are explained in the caption of Fig. 14.

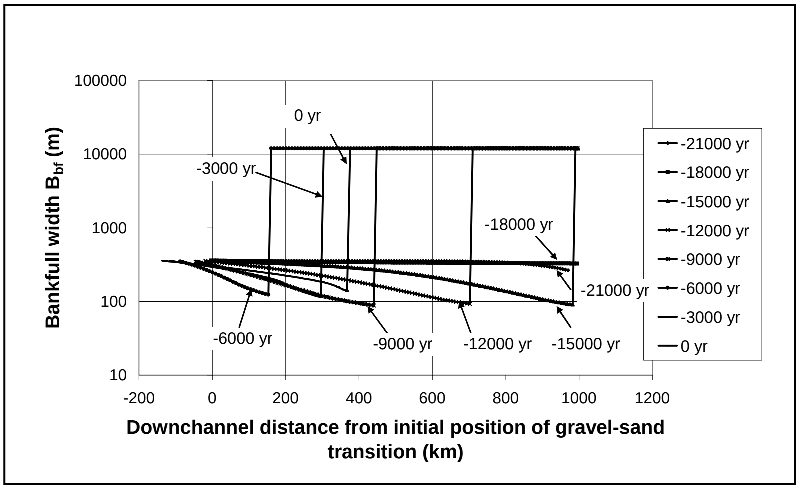

Fig. 12b. Profiles of bankfull width B_{bf} every 3000 years for Case B.

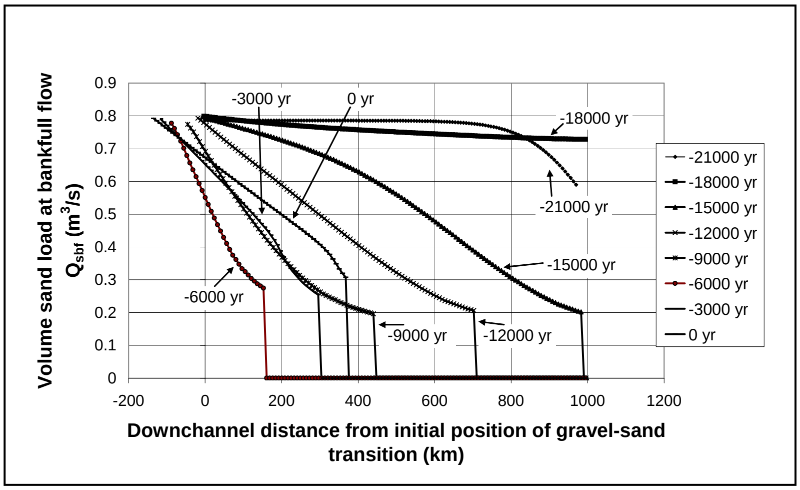

Fig. 12c. Profiles of volume sand transport rate at bankfull Q_{sbf} flow every 3000 years for Case B.

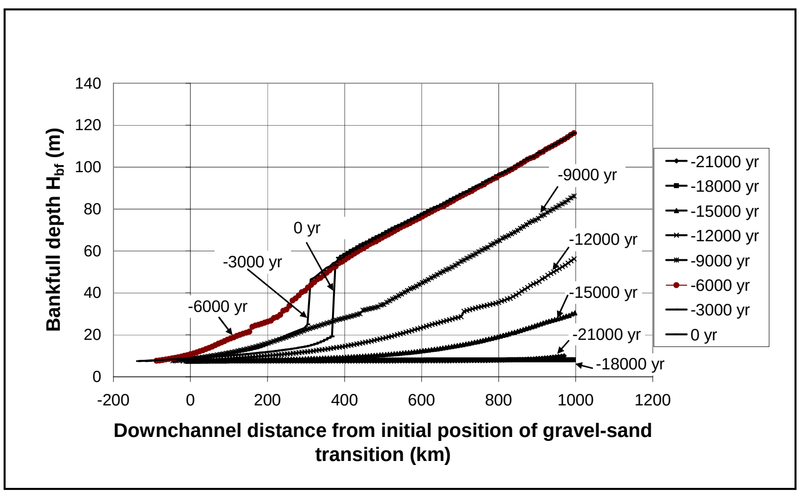

Fig. 12d. Profiles of bankfull depth H_{bf} every 3000 years for Case B.

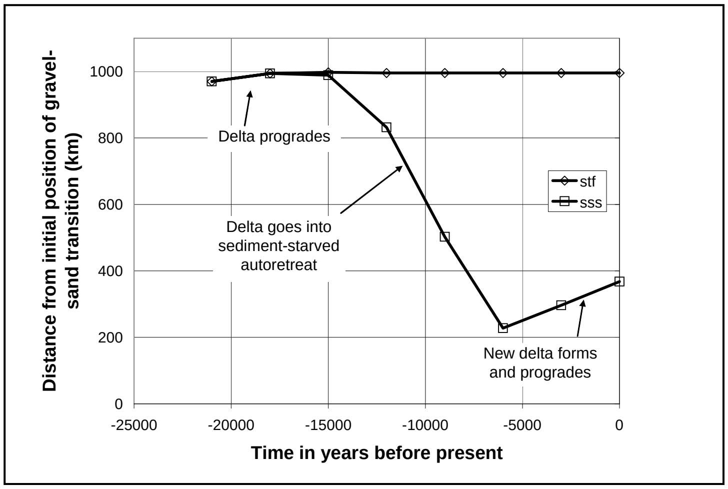

Fig. 12e. Plot of downchannel distance from the initial position of the gravel-sand transition to a) the delta topset-foreset break (stf) and b) the shoreline (sss) for Case B. The original delta is abandoned by – 15000 years; a new delta progrades outward after – 6000 years. By 0 years (present) the new delta has not yet merged with the abandoned delta.

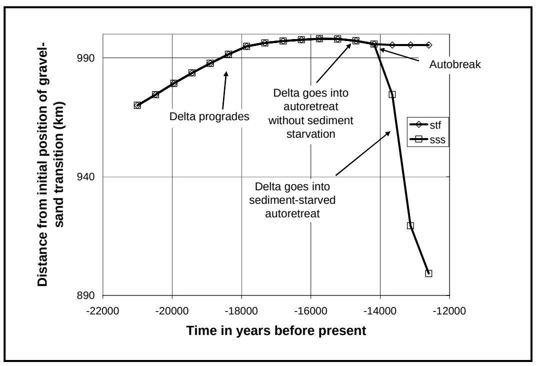

Fig. 12f. Expanded view of Fig. 25e showing the autobreak point for Case B.

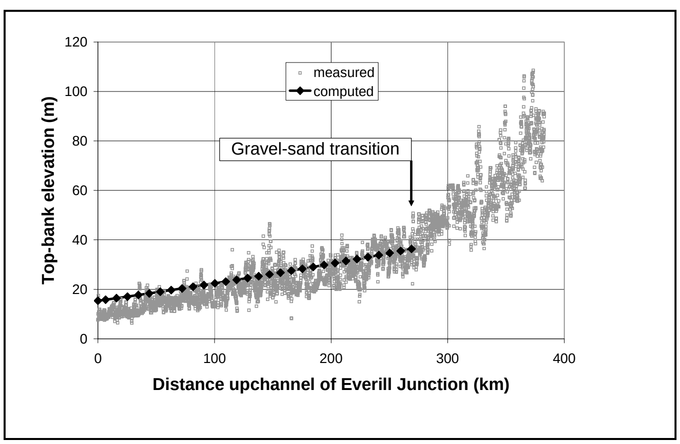

Fig. 12g. Plot showing the final computed bankfull water surface profile (0 years = present) of Case B from Everill Junction to the gravel-sand transition with SRTM data on bank elevation.

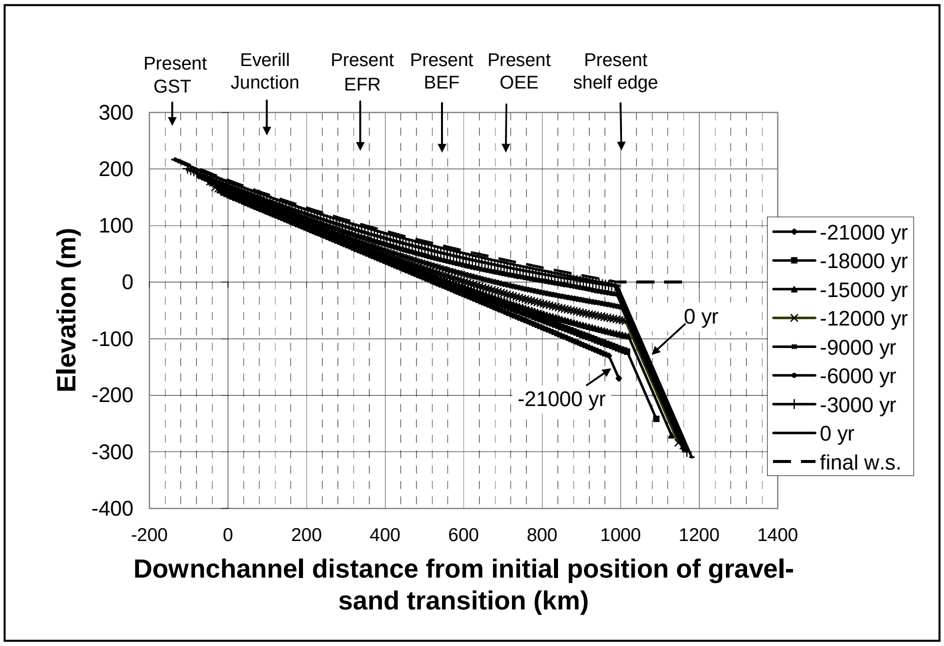

Fig. 13a. Profiles of bed elevation every 3000 years and final water surface elevation for Case C. The abbreviations “GST,” “EFR,” “BEF” and “OEE” are explained in the caption of Fig. 14.

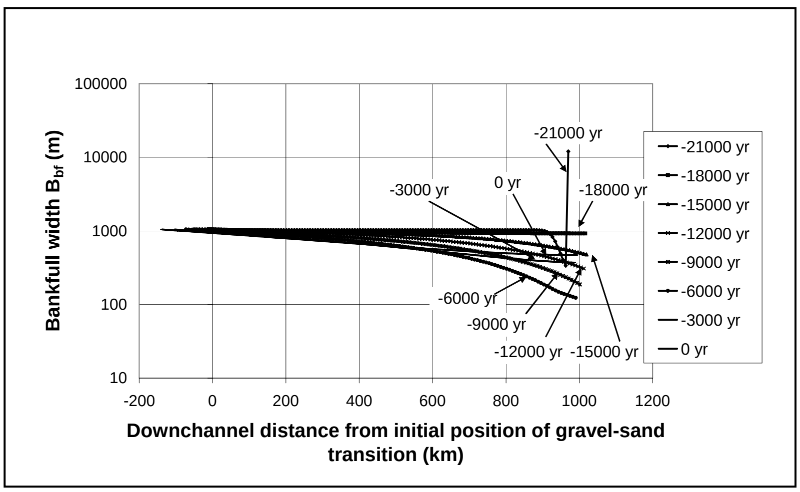

Fig. 13b. Profiles of bankfull width B_{bf} every 3000 years for Case C.

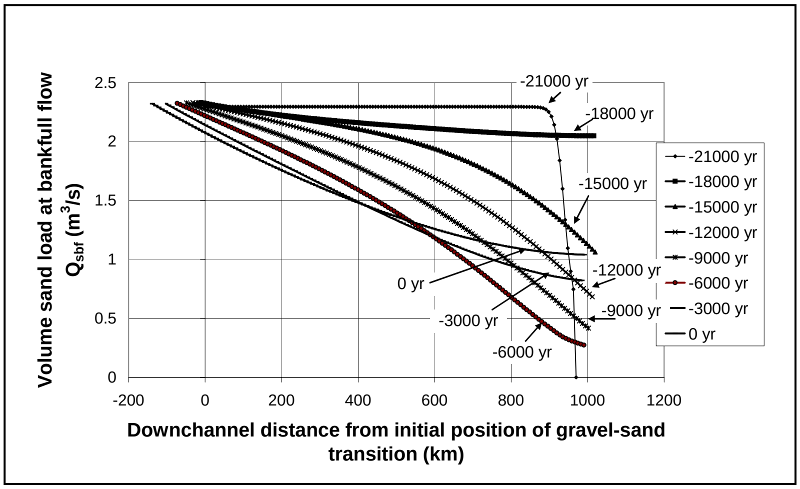

Fig. 13c. Profiles of volume sand transport rate at bankfull Q_{sbf} flow every 3000 years for Case C.

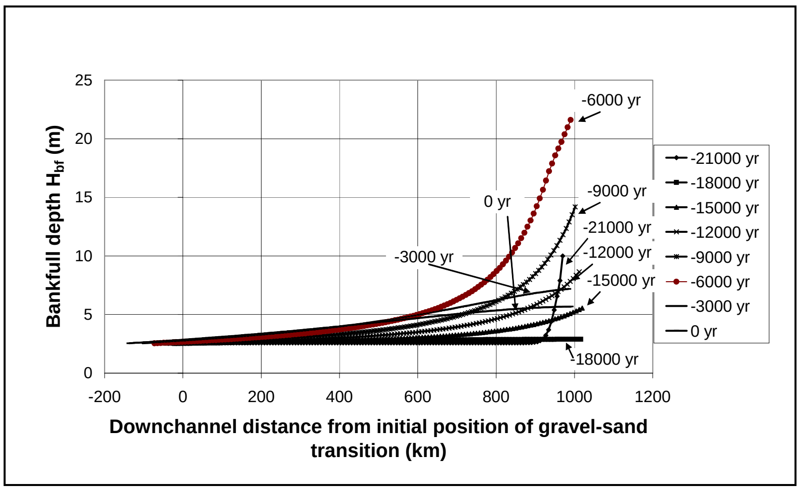

Fig. 13d. Profiles of bankfull depth H_{bf} every 3000 years for Case C.

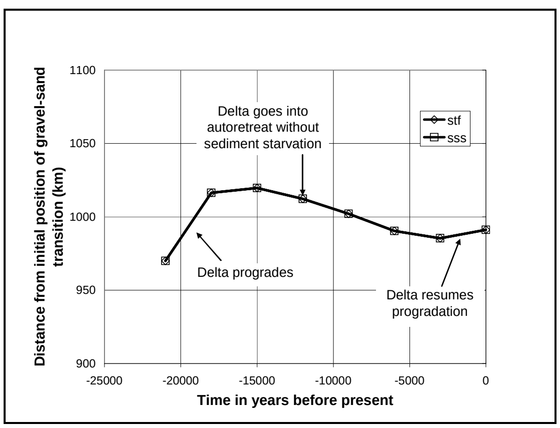

Fig. 13e. Plot of downchannel distance from the initial position of the gravel-sand transition to a) the delta topset-foreset break (stf) and b) the shoreline (sss) for Case C. The original delta is never abandoned by the shoreline in spite of 120 of sea level rise.

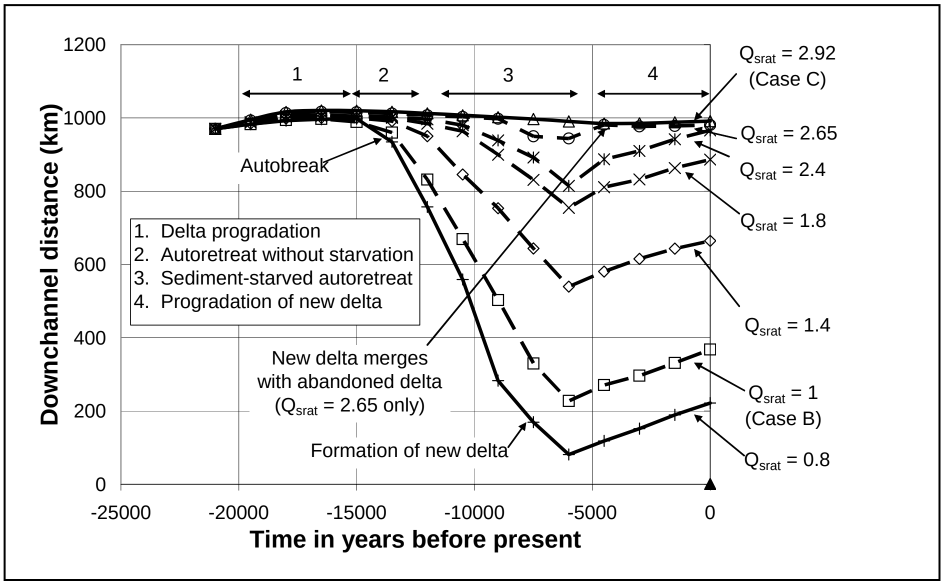

Fig. 14. Plot of downchannel distance from the initial position of the gravel-sand transition to the shoreline for seven cases. The parameters are the same as in Case B except that a) the sediment feed rate Q_{sbff} and initial fluvial slope S_{fi} of case B are both incremented by the seven factors Q_{srat} =0.8, 1 (Case B), 1.4, 1,8, 2,4, 2,65 and 2.92 (Case C).